EUROPEAN RESPIRATORY *journal*

FLAGSHIP SCIENTIFIC JOURNAL OF ERS

Early View

Original article

miR-184 mediates hyperoxia-induced injury by targeting cell death and angiogenesis signalling pathways in the developing lung

Dilip Shah, Karmyodh Sandhu, Pragnya Das, Zubair H. Aghai, Sture Andersson, Gloria Pryhuber, Vineet Bhandari

Please cite this article as: Shah D, Sandhu K, Das P, *et al*. miR-184 mediates hyperoxia-induced injury by targeting cell death and angiogenesis signalling pathways in the developing lung. *Eur Respir J* 2020; in press (https://doi.org/10.1183/13993003.01789-2019).

Expression of concern: Since the online publication of this early view article on 26 May 2020, the editors have been made aware of potential issues with some of the images used. This note has been added to make readers aware that this issue is currently being investigated by the editors and the authors. This note will be removed and a correction published, if found necessary by the investigation. The article was updated with this note and republished on 4 August, 2020.

miR-184 mediates hyperoxia-induced injury by targeting cell death and angiogenesis signaling pathways in the developing lung

Dilip Shah, PhD[1#], Karmyodh Sandhu, MS[1], Pragnya Das, PhD[1#], Zubair H. Aghai[2], Sture Andersson, MD, PhD[3], Gloria Pryhuber, MD[4], and Vineet Bhandari, MD, DM[1*#]

[1]Section of Neonatal-Perinatal Medicine, Department of Pediatrics, Drexel University College of Medicine, Philadelphia, PA, USA

[2]Division of Neonatology, Department of Pediatrics, Thomas Jefferson University Hospital, Philadelphia, PA, 19107, USA.

[3]Children's Hospital, University of Helsinki and Helsinki University Hospital, Helsinki, Finland

[4]Department of Pediatrics, University of Rochester School of Medicine and Dentistry, Rochester, NY, USA

Author Contributions: Conceived and designed—D.S., V.B; performed experiments—D.S., K.S., P.D., collected and analyzed the data—D.S., K.S., P.D., Z.A., S.A., G.P., V.B.; wrote manuscript—D.S., edited the manuscript— D.S., K.S., P.D., Z.A., S.A., G.P., V.B.; All authors have approved the version of the submitted manuscript.

Supported in part by departmental funds (D.S., P.D., and V.B.), Cure Grant (D.S), National Heart, Lung, and Blood Institute grant HL63039 and U01HL122700 (G.P.) from the National Institutes of Health, and a Finnish governmental subsidy for clinical research (S.A.).

Running title: *Role of miR-184 in Bronchopulmonary Dysplasia*

***Correspondence to**
Vineet Bhandari, MD, DM
Division of Neonatology
The Children's Regional Hospital at Cooper
One Cooper Plaza
Camden, NJ 08103
Off: 856-342-2000; extn: 1006156
Lab: 856-342-2000; extn: 1089752
Fax: 856-342-8007
E-mail: bhandari-vineet@cooperhealth.edu

[#]**Current Affiliation**: Neonatology Research Laboratory (Room #206), Education and Research Building, Cooper University Hospital, Camden, NJ

Abstract:

MicroRNAs (miRs) have been shown to disrupt normal lung development and function by interrupting alveolarization and vascularization leading to development of bronchopulmonary dysplasia (BPD). Here we report that miR-184 has a critical role in the induction of BPD phenotype characterized by abnormal alveolarization and pulmonary angiogenesis in the developing lung. We observed an increased expression of miR-184 in BPD clinical specimens: tracheal aspirates (TA), human neonatal lungs with BPD and in fetal human lung Type II alveolar epithelial cells (TIIAECs) exposed to hyperoxia. Consistent with this, we also detected an upregulated miR-184-3p expression in whole lungs, in freshly isolated TIIAECs from lungs of hyperoxia-induced experimental BPD mice and in fetal mice lung TIIAECs exposed to hyperoxia. We demonstrate that overexpression of miR-184-3p exacerbates the BPD pulmonary phenotype, while downregulation of miR-184-3p expression ameliorated the BPD phenotype and also improved respiratory function. We identified miR-184 specific targets: platelet-derived growth factor-beta (*Pdgf-β*) and friend of Gata 2 (*Fog2*), also known as zinc finger protein family member (*Zfpm2*), and show that they are critically involved in pulmonary alveolarization and angiogenesis. Using cell-based luciferase analysis, downregulation of miR-184-3p expression and gene knockdown of miR-184-3p targets Pdgf-β and Fog2 in lung TIIAECs and endothelial cells, we mechanistically show that inhibition of miR-184-3p expression improves pulmonary alveolarization by regulating PDGF-β/AKT/Foxo3/Bax, Bcl_2 signaling and enhances angiogenesis by Fog2/VEGF-A/Angiopoietin-1/2 pathway. Collectively, these data suggest that the use of miR-184-3p specific inhibitors may act as novel therapeutic interventions to control the adverse effects of hyperoxia on lung development and function.

Keywords: Hyperoxia, miR-184, AKT/FOXO3, VEGF-A, Angiogenesis, BPD

Introduction:

Bronchopulmonary dysplasia (BPD) is the most common chronic respiratory disease in infants and is a devastating condition that disrupts the developmental program of the lung secondary to preterm birth. BPD has been associated with a wide variety of risk factors (hyperoxia, invasive mechanical ventilation, and sepsis) [1, 2]. However, the histopathologic endpoints of this disease are the same — an impairment of alveolar development and dysregulated pulmonary vasculature. Pulmonary alveologenesis is a highly integrated process that implies cooperative interactions between interstitial, alveolar epithelial, and vascular compartments of the lung. It has been well established that hyperoxia exposure disrupts pulmonary alveolarization, impairs normal angiogenesis and endothelial vascular development [3]. These events in BPD lungs have been linked to aberrant expression of several key genes/proteins including vascular endothelial growth factor (VEGF, regulates angiogenesis), platelet-derived growth factor (PDGF, the requirement for elastin deposition and septation), and AKT (cell survival factor) in developing lungs [4-7]. Recent work from our lab and others have demonstrated the dynamic regulation of microRNAs (miRs) during lung development and deregulation of miRs have been reported in clinical [6, 8-10] and experimental (mice, rat, baboon) models of BPD [5, 6, 11, 12].

miRs are short endogenous RNA sequences (~22 nt) that mediate translational repression of target messenger RNAs (mRNAs), thereby inhibiting mRNA translation or promoting mRNA degradation (16). The mature miR species may be derived from both the 5' and 3' arms of the precursor duplex (pre-miR) and are called the miR-5p and -3p species, respectively. Increasing evidence from next-generation sequencing (NGS) studies have shown that half of the miR populations derived from mature miR species can co-exist as a miR-5p/-3p pair and both arms can be functional for altering their target mRNAs [13]. miRs have rapidly emerged not only as critically contributing to various pulmonary diseases [14, 15] but also to the normal development of the lung [11, 16]. The evidence that miRs play a role in lung development is derived from mice with conditional knockout of Dicer in lung epithelial cells that exhibited a failure of epithelial

branching, emphasizing the essential regulatory role of miRs in lung epithelial morphogenesis [17].

Our microarray study on the lungs of neonatal mice exposed to hyperoxia showed that miR-184 was one of the miRs which was over-expressed in hyperoxia-exposed developing lungs [6]. The miRbase sequence database analysis showed that human premiR184 exists as mature miR184, while in mouse the mature miR184 has been shown to co-exist as a miR-5p/-3p pair. Thus, we have systematically evaluated the expression of both 5p-arm and 3p-arm of miR184 in the murine hyperoxia-exposed experimental model of BPD and miR-184 expression in BPD clinical samples (human tracheal aspirates and lungs). We show that miR-184 expression was upregulated in the clinical samples (tracheal aspirates, lung tissues) obtained from human neonates with BPD. We also confirmed the increased expression of miR-184 in the lungs of hyperoxia-induced experimental BPD mice. Our *in-vivo* and *in-vitro* results show that hyperoxia upregulated miR-184-3p expression in experimental BPD mice lungs, in freshly isolated TIIAECs from the lungs of experimental BPD mice as well as in fetal lung TIIAECs exposed to hyperoxia. Interestingly we did not detect alteration of miR-184-5p in BPD mice lungs as well as fetal lung TIIAECs in response to hyperoxia. We hypothesized that upregulated miR-184-3p may affect the expression of its direct target proteins, friend of Gata 2 (Fog2) and PDGF beta (Pdgf-β) which deregulates their downstream proteins Akt, Forkhead box-O transcription factor 3 (Foxo1 and Foxo3), Vegf-A and contribute to abnormal alveolarization and dysregulated angiogenesis in the developing lung. Mechanistically we show that inhibition of miR-184-3p improved pulmonary alveolarization by regulating the Pdgf-β/Akt/Foxo3, Foxo1/Bax-Bcl_2 signaling pathway and enhanced endothelial angiogenesis by the Fog2/Vegf-A/Angiopoietin-1/2 pathway.

Materials and Methods

Human lung tracheal aspirates

The collection and processing of the lung tracheal aspirates (TA) from premature infants being mechanically ventilated in the first postnatal week with an indwelling endotracheal tube were approved by the human investigation committee (institutional review board) of Cooper University Hospital, and was done after obtaining consent (Z.A.) from one or both parents. Selected clinical details are provided in **Table E1** in the data supplement.

Human lung tissue

Collection and processing of the human lung samples after consent for expedited autopsy was done in a standardized manner as previously reported [18] (G.P.). Average post-mortem interval was 6.1 hours. This was approved by the University of Rochester Institutional Review Board. Selected clinical details are provided in **Table E2** in the data supplement.

Immunohistochemistry in human neonatal lungs

Details regarding the collection, processing and staining of the human lung sections with Pdgf-β antibody are described in the online data supplement.

Mouse studies

C57BL/6J Mice (Jackson Laboratory (Bar Harbor, ME) were housed and bred in Drexel University animal care facilities and allowed free access to standard food and water. All animal studies were approved by the Institutional Animal Care and Use Committee of Drexel University College of Medicine (Philadelphia, PA) prior to performing any studies.

Murine model of hyperoxia-induced experimental BPD

To generate the hyperoxia-induced murine experimental model of BPD, newborn mice were exposed to moderate hyperoxia (60% oxygen) from postnatal day 0 (PN0; saccular stage of

mouse lung development) to PN 4 (initiation of alveolar stage of mouse lung development) and then allowed to recover at room air (RA; 21% oxygen) till PN14 (alveolar stage), as previously described (8, 21, 22). Details are provided in the online data supplement.

miR-184-3p mimic and inhibitor experiments

Details are provided in the online data supplement.

Analysis of bronchoalveolar lavage (BAL) fluid

BAL was collected and total protein concentration in the BAL fluid was measured using the Pierce™ BCA assay kit (Fisher Scientific Co, Houston, TX), as previously described [18]. Details are provided in the online data supplement.

Enzyme-linked immunosorbent assay

Interleukin (IL)-6, IL-1β, and myeloperoxidase were quantified using commercially available DuoSet ELISA kits (R&D Systems) according to the manufacturer's instructions, as previously described [18].

Quantitative real-time PCR analysis

Details are provided in the online data supplement.

Cellular (Nuclear and cytoplasmic) fractionation

Details are provided in the online data supplement.

Western Blotting

Western blotting method, specific antibodies sources, and dilutions used are provided in the online data supplement.

Histological analysis

Details are provided in the online data supplement.

Lung morphometric analysis

Details are provided in the online data supplement.

Terminal deoxynucleotidy1 transferase-mediated dUTP nick end-labeling (TUNEL) assay

Details are provided in the online data supplement.

von Willebrand factor (VWF)

Pulmonary vessel density was determined based on immunofluorescence staining of vWF, an endothelial-specific marker, in the lung sections as described previously [19, 20]. Details are provided in the online data supplement.

Analysis of cell proliferation

Cell proliferation in the lungs of RA and experimental BPD mice treated with miR-184-inhibitor was studied by co-immunofluorescent detection of the proliferation marker Ki-67 (Red, Texas Red) [18]. Details are provided in the online data supplement.

Measurement of lung mechanics

Lung mechanics such as lung resistance, lung compliance, and tissue elastance were measured in anesthetized mice, as previously described [21]. Details are provided in the online data supplement.

Isolation of lung Type II AECs

Lung TIIAECs were isolated from murine lungs as per our earlier published method using MACS cell separation (Miltenyi Biotec, Spain) [22]. Please see the online data supplement for additional details.

Lung cell lines and cell culture

Details are provided in the online data supplement.

***In-vitro* overexpression and inhibition of miR-184-3p**

Details are provided in the online data supplement.

Luciferase assay:

Details are provided in the online data supplement.

Statistical analysis

Statistics were performed using GraphPad Prism 8.0 software (La Jolla, CA). The sample size was based on our previous publications [6, 18, 23]. Using chord length (describes the mean free distance in the air spaces in lungs) as the outcome of pulmonary alveolarization, we noted that this was abnormal in >99% of wild type (WT) BPD mice lungs. Using our targeted molecular therapy, we expected a 70% improvement. Hence, with an alpha=0.005, beta=0.2, and a power of 80%, we need n=6 in each group. Two-group comparisons were analyzed by the two-tailed unpaired Student's *t*-test and multiple-group comparisons were performed using one-way analysis of variance (ANOVA) followed by Tukey post hoc analysis. $P<0.05$ was considered statistically significant.

Results

Hyperoxia leads to increased miR-184 expression in the lungs of human and mice neonates with BPD.

To evaluate the potential role of miR-184 in hyperoxia-induced lung injury, abnormal alveolarization and pulmonary endothelial dysregulation in BPD lungs, we scrutinized the

relative expression of miR-184 in clinical specimens such as TA and lung tissues of human neonates with BPD. As shown in **Figures 1A**, the relative expression of miR-184 was significantly increased in TA of infants who subsequently developed BPD than in those who did not develop BPD. The detailed characterization of the enrolled infants is shown in **Table E1**. Similar to the increased level of miR-184 from TA from infants who subsequently developed BPD, miR-184 levels were higher in lung tissues from human neonates with BPD (**Figure 1B)** and in both male and female human fetal/neonatal lung TIIAECs exposed to hyperoxia at various time points (**Figure 1C**). The detailed characterization of this second independent cohort of enrolled infants (for data shown in **Figure 1B**) is shown in **Table E2**. Recently, some miRs have been reported to express differentially in experimental male and female BPD mice [23]. We observed that miR-184 was increased in human TA and in the lungs of both male and female neonates with BPD as compared to respective control groups, with no difference in the expression of miR-184 between male and female BPD neonates in TA as well as in lungs (**Supplementary Figure 1A-1D**).

We next evaluated the expression of miR-184 in a hyperoxia-induced murine model of experimental BPD. In mice, the mature miR184 has been shown to co-exist as a miR-5p/-3p pair, hence we first determined the relative expression of miR-184-3p and miR-184-5p in our *in vitro* and *in vivo* murine models of experimental BPD. As shown in **Supplementary Figure 2**, the expression of miR-184-5p did not significantly alter in lungs of experimental BPD mice as well as in fetal lung TIIAECs exposed to hyperoxia at various time points. Interestingly, the relative expression of miR-184-3p was significantly increased in lungs of hyperoxia-exposed newborn mice at postnatal day 4 (PN4), PN7 and PN14 (BPD) as compared to their respective control RA groups (**Figure 1D**). Also, we did not find a significant difference in the expression of miR-184-3p in male and female experimental BPD mice lungs (**Supplementary Figure 1E** and **1F**); thus, for the subsequent experiments, we have pooled both male and female neonatal

mice. As impaired alveolarization and pulmonary vascularization are the hallmarks of BPD, we consequently determined the level of miR-184-3p in fetal lung TIIAECs and in microvascular ECs exposed to hyperoxia. The expression of miR-184-3p was significantly increased in freshly isolated TIIAECs from the lungs of experimental BPD mice (**Figure 1E**) as well as in fetal mice lung TIIAECs exposed to hyperoxia at various time points (**Figure 1F**).

We lastly determined whether the miR-184 expression was also impacted in microvascular ECs. We noted that miR-184-3p expression was also upregulated in fetal mice lung ECs (**Figure 1G**) and in both male and female fetal/neonatal (28 weeks gestation) human lung ECs (**Figure 1H**) exposed to hyperoxia. Altogether, these data from hyperoxia-induced experimental BPD mice and two independent cohorts of human lung samples from neonates with BPD confirmed that miR-184 (-3p) is upregulated during hyperoxia exposure in developing lungs and may be associated with BPD development.

miR-184-3p exacerbates hyperoxia-induced lung injury and aberrant alveolarization in lungs

To ascertain the potential role of upregulated miR-184-3p in hyperoxia-induced lung injury and impaired alveolarization in neonatal lungs, we treated newborn mice with miR-184-3p mimic or scrambled mimic as a negative control and exposed them to hyperoxia as shown in **Supplementary Figure 3A**. We evaluated features of the BPD phenotype such as lung inflammation, pulmonary edema and alveolar simplification in these mice. We found that newborn mice treated with miR-184-3p mimic synergistically increased expression of miR-184-3p in lungs of RA and experimental BPD mice (**Figure 2A**). We did not find any significant changes in lung inflammation or the morphometric index of chord length when we compared RA to RA-scrambled mimic as well as BPD vs BPD scrambled mimic (**Supplementary Figures 3B, 3C**). Hence for subsequent experiments, we utilized RA and BPD as controls to compare with

miR-184-3p mimic experiments. Further, no change in mortality or growth (body weight) was noted in RA mice with and without transfection with miR-184-3p mimic (data not shown). We, however, observed increased lung inflammation and abnormal alveolarization in RA mice transfected with miR-184-3p mimic (**Supplementary Figures 3B and Figures 2B-2M**). These results suggest a role of miR-184-3p in the induction of the BPD pulmonary phenotype in mice. Further, the overexpression of miR-184-3p in BPD mice augmented total neutrophil recruitment into lungs (**Supplementary Figure 3B**) as well as exaggerated lung inflammation as evidenced by significantly enhanced levels of IL6 and IL1β in lungs as compared to experimental BPD mice (**Figures 2B-2D**). Increased lung inflammation by overexpression of miR-184-3p was also accompanied with compromised epithelial barrier function as indicated by reduced expression of tight junctions (TJs) proteins occludin and zonula occludens 1 (ZO-1) by western blots in lungs of experimental BPD mice (**Figure 2E**) as well as reduced immunofluorescence of ZO-1 in fetal lung TIIAECs transfected with miR184-3p mimic (**Figure 2F**). The decreased pulmonary epithelial barrier function by miR-184-3p mimic was further supported by increased total protein concentration in BAL fluid in experimental BPD mice transfected with miR-184-3p mimic (**Figure 2G**).

We next determined the consequence of overexpression of miR-184-3p in lung morphometric indices in these mice. As shown in **Figures 2H-2M**, overexpression of miR-184-3p in lungs of experimental BPD mice led to aberrant lung morphometry as evidenced by increased alveolar size measured as chord length, decreased radial alveolar counts (RAC), reduced number of junctions and branches in lungs. Taken together, these findings indicate that up-regulated miR-184-3p expression enhances the susceptibility to hyperoxia-induced lung injury and disrupts epithelial cell barrier function and pulmonary alveolarization in BPD.

Inhibition of miR-184-3p mitigates hyperoxia-induced lung inflammation

We found that the overexpression of miR-184-3p increases lung inflammation and disrupts pulmonary alveolarization. We next determined whether the inhibition of miR-184-3p expression in developing lungs mitigates hyperoxia-induced lung inflammation --- one of the major pathologic findings associated with BPD. The experimental plan is shown in **Figure 3A**. We found that newborn mice exposed to hyperoxia and treated with miR-184-3p inhibitor at PN1 and PN3 showed significantly diminished total immune cells (**Figure 3B**), neutrophil number in BAL fluid (**Figure 3C**) and myeloperoxidase activity in experimental BPD lungs (**Figure 3D**) as compared to experimental BPD mice treated with miR-184-3p scrambled. The miR-184-3p inhibitor mediated decreased lung inflammation was further supported by diminished levels of pro-inflammatory cytokines IL6 and IL1β measured by ELISA (**Figures 3E-3F**) and western blots (**Figure 3G**). We did not find any significant changes in lung inflammation when we compared RA to RA-scrambled inhibitor as well as experimental BPD vs experimental BPD scrambled inhibitor (**Figures 3B-3F**). Hence for subsequent experiments, we utilized RA and BPD as controls to compare with miR-184-3p inhibitor experiments.

We next ascertained whether decreased lung inflammation also correlates with decreased inflammation in TIIAECs. Consistent with reduced lung inflammation by miR-184-3p inhibitor in experimental BPD mice, we also noted the decreased levels of IL6 and IL1β in mice fetal lung TIIAECs transfected with miR-184-3p inhibitor and exposed to hyperoxia (**Figure 3H**). These data suggest that repressing miR-184-3p expression in lungs may ameliorate hyperoxia-induced lung inflammation.

Inhibition of miR-184-3p improves epithelial barrier function and pulmonary alveolarization in BPD lungs

To assess whether diminished lung inflammation by miR-184-3p inhibitor in neonatal lungs also influences the pulmonary epithelium injury and barrier function, we first evaluated the levels of

TJs proteins occludin and ZO-1 in mice fetal lung TIIAECs. We found occludin and ZO-1 levels were restored in mice fetal lung TIIAECs transfected with miR-184-3p inhibitor and exposed to hyperoxia (**Figure 4A and Figure 4B**). Similar to the *in-vitro* results, we observed that experimental BPD mice treated with miR-184-3p inhibitor also showed the increased levels of TJs proteins occludin and ZO-1 in lungs (**Figure 4C**). The improved pulmonary epithelial barrier function in lungs is further supported by decreased levels of total protein in the BAL fluid in experimental BPD mice treated with miR-184-3p inhibitor (**Figure 4D**). We also found that the improved pulmonary epithelial barrier by miR-184-3p inhibitor was also associated with improved overall lung morphometric indices in BPD mice (**Figure 4E-4J**). This is evident by decreased alveolar size measured as chord length (**Figure 4F**), increased RAC (**Figure 4G**), decreased septal thickness (**Figure 4H)**, increased number of branches (**Figure 4I**) and junctions (**Figure 4J**) in the lungs of experimental BPD mice treated with miR-184 inhibitor. Taken together, these findings indicate that inhibition of miR-184-3p expression attenuates hyperoxia-induced lung inflammation, injury, improves epithelial cell barrier function and pulmonary alveolarization in experimental BPD mice.

miR-184-3p improves pulmonary alveolarization by regulating *Pdgf-β*/Akt/Foxo3, Foxo1/Bax, Bcl_2 signaling

We next investigated the mechanism by which upregulated miR-184-3p expression in response to hyperoxia impaired pulmonary alveolarization and angiogenesis in BPD. Accumulated evidence indicates that miRs are engaged in posttranscriptional regulation of biological processes including cell proliferation, angiogenesis, and apoptosis in developing lungs [5, 6, 11, 12, 24]. To determine miR-184-3p targets and uncover the mechanism that affects lung development in BPD, we performed a bioinformatics analysis of the miR-184-3p databases [miRTARbase [25] and TargetScan [26]]. Bioinformatics analysis showed that mmu-miR184-3p has 49 conserved targets. Since it was not feasible to evaluate all possible targets, we selected

to evaluate two important genes; *Pdgf-β* and *Fog2* (ZFPM2) which have been shown to be involved in the regulation of the cell survival factor AKT, and VEGF signaling (angiogenesis) in developing lungs [4, 5]. We noted that Fog2 and Pdgf-β levels and staining were significantly decreased in lung tissues of human neonates with BPD as compared to term controls (**Figure 5A and Supplementary Figure 4A**) as well as in experimental BPD mice lungs (**Supplementary Figures 4B-4C**) and in TIIAECs (**Figure 5C**), indicating that the decreased Pdgf-β and Fog2 levels may be related to upregulated miR-184-3p expression in these lungs. The detailed characterization of the enrolled infants is shown in **Table E3**. We further confirmed Pdgf-β and Fog2 as the direct targets of miR-184-3p, by performing cell-based luciferase assays. As shown in **Figure 5B** and **Supplementary Figure 5A,** Pdgf-β and Fog2 are the bona fide targets of miR-184-3p which are consistent with an earlier report on human limbal epithelial keratinocytes (HLEKs) [27]. Consistent with the luciferase results, we also found that inhibition of miR-184-3p expression upregulated Pdgf-β and Fog2 levels in mice fetal lung TIIAECs *in vitro* (**Figure 5C**) and *in vivo* (in whole lungs of experimental BPD mice) exposed to hyperoxia (**Figure 5D**). To confirm the reporter analysis, we overexpressed miR184-3p in cells and mice lungs. As shown in **Supplementary Figures 5B and 5C**, overexpression of miR-184-3p significantly reduced levels of Pdgf-β and Fog2 in fetal lung TIIAECs, ECs and in experimental BPD mice lungs. Having established Pdgf-β and Fog2 as the direct targets of miR-184-3p, we sought to elucidate the role of these proteins in lung development in hyperoxia conditions. It is known that Pdgf-β activates cell survival AKT signaling [27, 28]; thus, we next measured AKT activity in response to hyperoxia in the presence or absence of miR-184-3p inhibitor and mimic. As shown in **Supplementary Figures 6A and 6B**, AKT activity (denoted by p-AKT expression) was decreased by miR-184-3p mimic, while its activity was increased by miR-184-3p inhibitor in lung TIIAECs (**Figure 5E)** as well as in lungs of experimental BPD mice (**Figure 5F)**. We confirmed the regulatory effect of Pdgf-β on AKT expression by knockdown of *Pdgf-β* gene in lung TIIACECs followed by exposure to hyperoxia. The knockdown of *Pdgf-β* gene showed the

decreased expression of p-AKT and confirmed the stimulatory effect of Pdgf-β on AKT activity in lung TIIAECs (**Figures 5G**). Several earlier studies have demonstrated that activated AKT can enhance cell survival by phosphorylating numerous downstream targets including forkhead family (Foxo) transcription factors and bcl-2 family members [29, 30]. We found that direct phosphorylation by AKT inhibited the transcriptional activation by Foxo factors; p-Foxo1 (Ser319) and p-Foxo3 (Ser253), causing their displacement from the nucleus into the cytosol as an inactive state (**Figure 6A**). We next explored the role of Foxo-mediated apoptosis in BPD mice treated with miR-184-3p mimic and inhibitor. As shown in **Supplementary Figures 7A and 7B,** the expression of pro-survival protein Bcl_2 level was decreased, while pro-apoptotic protein Bax and TUNEL staining were increased in lungs of BPD mice treated with miR184 mimic. Consistent with the mimic results, miR-184-3p inhibitor showed an augmented level of Bcl_2, a decreased level of Bax and a reduced level of cleaved caspase-3 in experimental BPD mice lungs (**Figure 6B**) and fetal lung TIIAECs (**Figure 6C**) as well as lower TUNEL staining in lungs of experimental BPD mice (**Figure 6D and Supplementary Figure 8A**). Furthermore, the decrease in lung cell death was also associated with increased cell proliferation in BPD lungs as noted by increased staining of ki67 in lungs of experimental BPD mice treated with miR-184-3p inhibitor (**Figure 6E and Supplementary Figure 8B**). These results indicate that inhibition of miR-184-3p expression in response to hyperoxia exerts the protective effects and attenuates apoptosis via PDGF-β/AKT/Foxo3/Bax, Bcl_2 signaling pathway.

miR-184-3p mitigates pulmonary angiogenesis by targeting Fog2/Vegf-A/Ang-1pathway

We next evaluated the role of another important miR-184-3p target, Fog2, in BPD. Fog2 is known to be essential for heart morphogenesis and coronary development [31, 32]. Its function in lung development in response to hyperoxia has not been investigated. Fog2 has been shown to potentially affect angiogenesis by promoting the expression of Vegf [33]. We found that Fog2 level was decreased in human fetal lung ECs exposed to hyperoxia and miR-184-3p mimic

further decreased its level (**Supplementary Figure 9A**), while miR-184-3p inhibitor restored the level of Fog2 in human fetal lung ECs (**Supplementary Figure 9B**). Further, we noted that miR-184-3p mimic-mediated decreased Fog2 expression was related to reduced level of VEGF-A in experimental BPD lungs (**Supplementary Figure 10A**). Similarly, mice fetal lung ECs and experimental BPD mice treated with miR-184-3p inhibitor rescued the deceased level VEGF-A in lung ECs (**Figure 7A**) and in whole lung tissues (**Figure 7B**). We confirmed the regulatory effect of Fog2 on VEGF-A expression by knockdown of Fog2 gene in lung ECs followed by exposure to hyperoxia. The knockdown of Fog2 gene showed the decreased expression of VEGF-A and confirmed the stimulatory effect of Fog2 on VEGF-A expression in lung ECs (**Supplementary Figure 10B**). Further, we found that decreased expression of VEGF-A was associated with deregulated angiogenesis with an increased level of Ang2 and decreased level of Ang1 in lung ECs and in experimental BPD lungs treated with miR-184-3p mimic (**Supplementary Figure 10A**), whereas miR-184-3p inhibitor improved angiogenesis in lung ECs and in BPD lungs (**Figures 7A and 7B**). Notably we found that the improved lung angiogenesis by miR-184-3p inhibitor was also concomitant with improved vascularization in lungs of experimental BPD mice treated with miR-184-3p inhibitor (**Figure 7C and Supplementary Figure 11**). Collectively, these data suggest that miR-184-3p mitigates pulmonary angiogenesis and vascularization by targeting Fog2/Vegf-A/Ang-1 pathway.

Enhanced pulmonary alveolarization and endothelial angiogenesis by inhibition of miR-184-3p are associated with improved lung mechanics in BPD

Lastly, we determined whether miR-184-3p inhibitor-mediated improved pulmonary alveolarization and angiogenesis also improves lung mechanics in experimental BPD mice. We measured lung mechanics parameters such as lung resistance, elastance, and compliance in RA and experimental BPD mice treated with miR-184-3p inhibitor and mimic. As shown in **Figure 7D-7F**, miR-184-3p inhibitor improved lung mechanics in experimental BPD mice as

manifested by diminished lung resistance and elastance with enhanced lung compliance as compared to non-treated BPD group. Consistent with these results, miR-184-3p mimic exacerbated lung mechanics parameters such as lung resistance, elastance, and compliance in experimental BPD mice (**Supplementary Figures 10C-10E**). Importantly, we noted a worse BPD phenotype in RA mice treated with miR-184-3p mimic as this was accompanied by altered lung mechanics parameters such as lung resistance, elastance, and compliance. Overall our results suggest that deregulated miR-184-3p expression in neonatal lung impaired lung development and compromised the physiological function of lung. **Figure 7G** shows a diagram of our proposed hypothesis and results.

Discussion:

miR-184 is abundantly expressed in neonatal lungs in response to hyperoxia; however, its physiological and pathologic functions in lung development are largely unknown. We report here that miR-184-3p expression is increased in lung tissues, in TIIAECs, and in ECs in an experimental murine model of BPD as well as in clinical specimens (TA and lung tissues) obtained from human neonates with BPD. We demonstrated that hyperoxia-induced altered miR-184-3p expression deregulated expression of its target proteins PDGF-β in lung TIIAECs and Fog2 in lung ECs and overall these effects led to compromised lung development and physiological function of lungs. Further, we provided the evidence for a novel role of deregulated PDGF-β in AKT/Foxo3-mediated abnormal alveolarization and Fog2 in VEGF-A-mediated impaired vascularization in BPD lungs. This novel insight may help to clarify some of the mechanisms underlying hyperoxia-induced abnormal alveolarization/dysregulated vascularization in human BPD (with the caveat that human BPD is contributed to by additional genetic-environmental factors for e.g. invasive mechanical ventilation) and reveal new possible targets for treating lung abnormalities induced by hyperoxia.

Pulmonary alveologenesis is a highly integrated process that implies cooperative interactions between interstitial, alveolar epithelial, and vascular compartments of the lung. It is well established that prolonged hyperoxia exposure deregulated several important genes which are required for normal lung development [3, 6]. Recently, multiple studies demonstrated that miRs such as miR-17~92 cluster, miR-29b, miR-30a, miR-34a, miR-421, miR-489, and miR 876-3p were altered in neonatal lungs in response to hyperoxia and deregulated the progress of BPD development. These miRs mediated events included modulation of lung cell proliferation/differentiation, apoptosis, alveolarization, angiogenesis and vascularization in lungs [5, 6, 9, 12, 24, 34], thus becoming a research hotspot in studying the roles of miRs in lung development/injury. Here, we demonstrated that hyperoxia-induced miR-184-3p expression in neonatal lungs led to deregulation of at least two important proteins, PDGF-β and Fog2, which were directly related to disruption of normal alveolarization and angiogenesis in BPD lungs and had cumulative effects on compromised normal lung development and function.

PDGF signaling regulates numerous events such as cell proliferation, differentiation, migration, and survival, suggesting its crucial role in the embryonic and early stage of lung development [35, 36]. Five different isoforms (PDGF-AA, PDGF-BB, PDGF-CC, PDGF-DD, and PDGF-AB) and two PDGF-receptor isotypes (PDGFRα and PDGFRβ) have been described and abundantly found in most cell types in lungs [37]. Among these isoforms, PDGF-AA (PDGF-α) and its receptor PDGFRα have been well studied in lung development and in BPD [37]; however, little is known about the role of PDGF-BB (PDGF-β). Our results showed that PDGF-β is abundantly present in neonatal lungs and lung TIIAECs and its level decreased with hyperoxia exposure in our experimental murine model of BPD as well as in lung tissues of human neonates with BPD.

We used cell-based luciferase assays, miR-184-3p mimic and inhibitor in lung TIIAECs and BPD mice and showed that miR-184-3p directly regulate expression of PDGF-β in lungs and in TIIAECs. These reports are also supported by an earlier study [27]. In addition, we noted that

restoration of PDGF-β levels by downregulating miR-184 expression led to decreased cell death, suggesting a pro-survival activity of PDGF-β in neonatal lungs. Previous reports have demonstrated that PDGF-β promotes AKT activity [38, 39] and we have earlier reported that AKT is an important kinase mediating the survival response in newborn mice exposed to hyperoxia [6]. Thus, we speculate that decreased cell death may be due to increased AKT activity and its downstream signaling to inhibit apoptosis in lungs of experimental BPD mice treated with miR-184 inhibitor. We show that the pro-survival effects of PDGF-β are mediated by AKT phosphorylation (Thr308) and subsequent Foxo1(Ser253) and Foxo3 phosphorylation (Ser253). Our mechanistic data showed that AKT inhibits transcriptional functions of Foxo1 and Foxo3 by phosphorylating and translocating them from the nucleus to cytoplasm thus sequestering Foxos away from the promoters of apoptotic genes and supports TIIAECs survival, growth and proliferation in BPD lungs. Consistent with our report, the reduced Foxo1,o3 phosphorylation has been shown to correlate with decreased longevity and increased apoptosis in several previous studies [29, 40]. Although we are the first to demonstrate the role of Foxo1 and Foxo3 in BPD development, there are certain limitations to our report. We have not extensively explored the specific mechanism of Foxo1 and Foxo3 in Bcl_2/Bax-mediated apoptosis in lungs and further studies are required to provide complete mechanistic insight.

Another important finding of this study is that we illustrated, for the first time, to our knowledge, that proangiogenic factor friend of Gata 2 (Fog2) is involved in the regulation of ECs angiogenesis in BPD lungs through augmentation of VEGF-A expression. An earlier study has shown that Fog2 is critical for the development of normal pulmonary lobar structure [41] and Fog2 mutation in mice results in pulmonary lobar defects [42]; however, its role in neonatal lung development has not been explored. To understand the relevant role of Fog2 in BPD, we measured its level in the lung tissues of human neonates with BPD and their matched controls. We found that Fog2 level was decreased in lung tissues with BPD indicating that Fog2

expression may be related to the BPD phenotype. We subsequently demonstrated that miR-184-3p negatively regulates expression of Fog2 in lung ECs and modulates ECs angiogenesis by targeting VEGF-A expression. Using a luciferase reporter assay, we show that Fog2 is a bona-fide miR-184 target [27] and promotes the expression of VEGF. VEGF signaling plays a major role for microvascular lung development. Among the VEGF proteins, VEGF-A is a potent angiogenic factor and decreased level of VEGF-A has been reported in lungs of preterm infants with fatal BPD [43]. Furthermore, recombinant human VEGF treatment has been recognized to promote angiogenesis to prevent BPD in newborn rats [44]. We have previously shown that VEGF-A promotes angiogenesis by decreasing expression of Ang2 and increasing expression of Ang1 in experimental BPD lungs [45, 46]. Consistent with these reports, we found that miR-184-inhibitor mediated increased VEGF-A expression promotes angiogenesis by decreasing Ang2/Ang1 ratio in lung ECs. Even though our results clearly suggest that Fog2-mediated improved lung endothelium angiogenesis through VEGF-A/Ang-1/2 pathway, there could be other pathways also involved. It is possible that Fog2 interacted with Gata4 to mediate the improvement of angiogenesis as an earlier study has shown that Fog2–Gata4 interactions mediated the later lung development including pulmonary vascular development and function [42]. An extensive evaluation of both Fog2 and Gata4 expression in lung endothelium in BPD mice will help to answer these questions.

Importantly, we demonstrated that lung mechanical parameters such as lung resistance, elastance, and compliance were improved in experimental BPD mice because of enhanced pulmonary alveolarization, angiogenesis and vascularization in lungs which were mediated by downregulation miR-184 expression. This study was based on evaluating the effects of miR-184 direct targets (Pdgf-β and Fog2) on pulmonary alveolarization and angiogenesis using miR-184-3p mimic and inhibitor in fetal lung TIIAECs, ECs and hyperoxia based experimental murine model of BPD. It will be interesting to test whether lung cells specific overexpression or

downregulation of miR-184-3p targets (Pdgf-β and Fog2) will also show similar effects, as we reported above, to determine the specificity of our findings.

We and others have recently reported that some miRs such as miR-30a, miR-34a and miR-146 were expressed differentially in experimental male and female BPD mice lungs [23, 34]. We noted that miR-184 expression was higher in both male and female human BPD samples (TA and lungs) as well as I n lungs of experimental BPD mice. However, we did not observe a significant difference in miR-184 expression in male versus female lung BPD samples. We acknowledge certain limitations in our study as well. It is possible that miR-184 may modulate pulmonary alveolarization and endothelial dysfunction through other known targets such as phosphatidic acid phosphatase type 2B (PPAP2B), hypoxia-inducible factor (HIF)-1 and epidermal growth factor (EGF) pathways involved in regulating directional migration of myofibroblasts and may contribute to impaired alveolar development in BPD [27, 47, 48]. The other limitation is this study is primarily focused on the lung TIIAECs and ECs; we recognize that miR-184 may affect additional cell types within the lung, including lung TIAECs and immune cells, such as macrophages. miR-184 has not been reported in human skin fibroblasts [49]. Relevant to the role of miR-184 in BPD, it would be interesting to know whether miR-184 also changes in lung cell types in response to mechanical stretch forces, an important factor for fetal alveolar epithelial cell differentiation [50].

In summary, our results show that the use of miR-184 specific inhibitors or pharmacological modulators of PDGF-β and Fog2 may act as new therapeutic interventions to control the adverse effects of hyperoxia in lung development and function.

References:

1. Bhandari A, Bhandari V. "New" Bronchopulmonary Dysplasia: A clinical review. *Clin Pulm Med* 2011: 18(3): 137-143.
2. Jensen EA, Schmidt B. Epidemiology of bronchopulmonary dysplasia. *Birth defects research Part A, Clinical and molecular teratology* 2014: 100(3): 145-157.
3. Berger J, Bhandari V. Animal models of bronchopulmonary dysplasia. The term mouse models. *Am J Physiol Lung Cell Mol Physiol* 2014: 307(12): L936-947.
4. Alphonse RS, Vadivel A, Coltan L, Eaton F, Barr AJ, Dyck JR, Thebaud B. Activation of Akt protects alveoli from neonatal oxygen-induced lung injury. *Am J Respir Cell Mol Biol* 2011: 44(2): 146-154.
5. Ruiz-Camp J, Quantius J, Lignelli E, Arndt PF, Palumbo F, Nardiello C, Surate Solaligue DE, Sakkas E, Mizikova I, Rodriguez-Castillo JA, Vadasz I, Richardson WD, Ahlbrecht K, Herold S, Seeger W, Morty RE. Targeting miR-34a/Pdgfra interactions partially corrects alveologenesis in experimental bronchopulmonary dysplasia. *EMBO Mol Med* 2019: 11(3).
6. Syed M, Das P, Pawar A, Aghai ZH, Kaskinen A, Zhuang ZW, Ambalavanan N, Pryhuber G, Andersson S, Bhandari V. Hyperoxia causes miR-34a-mediated injury via angiopoietin-1 in neonatal lungs. *Nat Commun* 2017: 8(1): 1173.
7. Bhandari V. Postnatal inflammation in the pathogenesis of bronchopulmonary dysplasia. *Birth defects research Part A, Clinical and molecular teratology* 2014: 100(3): 189-201.
8. Wu YT, Chen WJ, Hsieh WS, Tsao PN, Yu SL, Lai CY, Lee WC, Jeng SF. MicroRNA expression aberration associated with bronchopulmonary dysplasia in preterm infants: a preliminary study. *Respiratory care* 2013: 58(9): 1527-1535.
9. Olave N, Lal CV, Halloran B, Pandit K, Cuna AC, Faye-Petersen OM, Kelly DR, Nicola T, Benos PV, Kaminski N, Ambalavanan N. Regulation of alveolar septation by microRNA-489. *Am J Physiol Lung Cell Mol Physiol* 2016: 310(5): L476-487.
10. Lal CV, Olave N, Travers C, Rezonzew G, Dolma K, Simpson A, Halloran B, Aghai Z, Das P, Sharma N, Xu X, Genschmer K, Russell D, Szul T, Yi N, Blalock JE, Gaggar A, Bhandari V, Ambalavanan N. Exosomal microRNA predicts and protects against severe bronchopulmonary dysplasia in extremely premature infants. *JCI Insight* 2018: 3(5).
11. Nardiello C, Morty RE. MicroRNA in late lung development and bronchopulmonary dysplasia: the need to demonstrate causality. *Molecular and cellular pediatrics* 2016: 3(1): 19.
12. Bhaskaran M, Xi D, Wang Y, Huang C, Narasaraju T, Shu W, Zhao C, Xiao X, More S, Breshears M, Liu L. Identification of microRNAs changed in the neonatal lungs in response to hyperoxia exposure. *Physiol Genomics* 2012: 44(20): 970-980.
13. Yang JS, Phillips MD, Betel D, Mu P, Ventura A, Siepel AC, Chen KC, Lai EC. Widespread regulatory activity of vertebrate microRNA* species. *RNA* 2011: 17(2): 312-326.
14. Angulo M, Lecuona E, Sznajder JI. Role of MicroRNAs in lung disease. *Archivos de bronconeumologia* 2012: 48(9): 325-330.
15. Pagdin T, Lavender P. MicroRNAs in lung diseases. *Thorax* 2012: 67(2): 183-184.
16. Ameis D, Khoshgoo N, Iwasiow BM, Snarr P, Keijzer R. MicroRNAs in Lung Development and Disease. *Paediatric respiratory reviews* 2017: 22: 38-43.

17. Harris KS, Zhang Z, McManus MT, Harfe BD, Sun X. Dicer function is essential for lung epithelium morphogenesis. *Proceedings of the National Academy of Sciences of the United States of America* 2006: 103(7): 2208-2213.
18. Syed MA, Shah D, Das P, Andersson S, Pryhuber G, Bhandari V. TREM-1 Attenuates RIPK3 Mediated Necroptosis in Hyperoxia Induced Lung Injury in Neonatal Mice. *Am J Respir Cell Mol Biol* 2018.
19. Kato T, Kimura T, Ishii N, Fujii A, Yamamoto K, Kameoka S, Nishikawa T, Kasajima T. The methodology of quantitation of microvessel density and prognostic value of neovascularization associated with long-term survival in Japanese patients with breast cancer. *Breast Cancer Res Treat* 1999: 53(1): 19-31.
20. Shikata F, Sakaue T, Nakashiro K, Okazaki M, Kurata M, Okamura T, Okura M, Ryugo M, Nakamura Y, Yasugi T, Higashiyama S, Izutani H. Pathophysiology of lung injury induced by common bile duct ligation in mice. *PLoS One* 2014: 9(4): e94550.
21. James ML, Ross AC, Nicola T, Steele C, Ambalavanan N. VARA attenuates hyperoxia-induced impaired alveolar development and lung function in newborn mice. *Am J Physiol Lung Cell Mol Physiol* 2013: 304(11): L803-812.
22. Romero F, Shah D, Duong M, Penn RB, Fessler MB, Madenspacher J, Stafstrom W, Kavuru M, Lu B, Kallen CB, Walsh K, Summer R. A pneumocyte-macrophage paracrine lipid axis drives the lung toward fibrosis. *Am J Respir Cell Mol Biol* 2015: 53(1): 74-86.
23. Leary S, Das P, Ponnalagu D, Singh H, Bhandari V. Genetic Strain and Sex Differences in a Hyperoxia-Induced Mouse Model of Varying Severity of Bronchopulmonary Dysplasia. *Am J Pathol* 2019: 189(5): 999-1014.
24. Durrani-Kolarik S, Pool CA, Gray A, Heyob KM, Cismowski MJ, Pryhuber G, Lee LJ, Yang Z, Tipple TE, Rogers LK. miR-29b supplementation decreases expression of matrix proteins and improves alveolarization in mice exposed to maternal inflammation and neonatal hyperoxia. *American journal of physiology Lung cellular and molecular physiology* 2017: 313(2): L339-L349.
25. Lu TP, Lee CY, Tsai MH, Chiu YC, Hsiao CK, Lai LC, Chuang EY. miRSystem: an integrated system for characterizing enriched functions and pathways of microRNA targets. *PloS one* 2012: 7(8): e42390.
26. Agarwal V, Bell GW, Nam JW, Bartel DP. Predicting effective microRNA target sites in mammalian mRNAs. *eLife* 2015: 4.
27. Park JK, Peng H, Yang W, Katsnelson J, Volpert O, Lavker RM. miR-184 exhibits angiostatic properties via regulation of Akt and VEGF signaling pathways. *FASEB J* 2017: 31(1): 256-265.
28. Zhang H, Bajraszewski N, Wu E, Wang H, Moseman AP, Dabora SL, Griffin JD, Kwiatkowski DJ. PDGFRs are critical for PI3K/Akt activation and negatively regulated by mTOR. *The Journal of clinical investigation* 2007: 117(3): 730-738.
29. Katsoulieris EN, Drossopoulou GI, Kotsopoulou ES, Vlahakos DV, Lianos EA, Tsilibary EC. High Glucose Impairs Insulin Signaling in the Glomerulus: An In Vitro and Ex Vivo Approach. *PLoS One* 2016: 11(7): e0158873.
30. Obrador-Hevia A, Serra-Sitjar M, Rodriguez J, Villalonga P, Fernandez de Mattos S. The tumour suppressor FOXO3 is a key regulator of mantle cell lymphoma proliferation and survival. *British journal of haematology* 2012: 156(3): 334-345.

31. Svensson EC, Huggins GS, Lin H, Clendenin C, Jiang F, Tufts R, Dardik FB, Leiden JM. A syndrome of tricuspid atresia in mice with a targeted mutation of the gene encoding Fog-2. *Nat Genet* 2000: 25(3): 353-356.
32. Tevosian SG, Deconinck AE, Tanaka M, Schinke M, Litovsky SH, Izumo S, Fujiwara Y, Orkin SH. FOG-2, a cofactor for GATA transcription factors, is essential for heart morphogenesis and development of coronary vessels from epicardium. *Cell* 2000: 101(7): 729-739.
33. Zhou B, Ma Q, Kong SW, Hu Y, Campbell PH, McGowan FX, Ackerman KG, Wu B, Zhou B, Tevosian SG, Pu WT. Fog2 is critical for cardiac function and maintenance of coronary vasculature in the adult mouse heart. *J Clin Invest* 2009: 119(6): 1462-1476.
34. Zhang Y, Coarfa C, Dong X, Jiang W, Hayward-Piatkovskyi B, Gleghorn JP, Lingappan K. MicroRNA-30a as a candidate underlying sex-specific differences in neonatal hyperoxic lung injury: implications for BPD. *Am J Physiol Lung Cell Mol Physiol* 2019: 316(1): L144-L156.
35. Bostrom H, Willetts K, Pekny M, Leveen P, Lindahl P, Hedstrand H, Pekna M, Hellstrom M, Gebre-Medhin S, Schalling M, Nilsson M, Kurland S, Tornell J, Heath JK, Betsholtz C. PDGF-A signaling is a critical event in lung alveolar myofibroblast development and alveogenesis. *Cell* 1996: 85(6): 863-873.
36. Gouveia L, Betsholtz C, Andrae J. PDGF-A signaling is required for secondary alveolar septation and controls epithelial proliferation in the developing lung. *Development* 2018: 145(7).
37. Noskovicova N, Petrek M, Eickelberg O, Heinzelmann K. Platelet-derived growth factor signaling in the lung. From lung development and disease to clinical studies. *American journal of respiratory cell and molecular biology* 2015: 52(3): 263-284.
38. Li L, Xu M, Li X, Lv C, Zhang X, Yu H, Zhang M, Fu Y, Meng H, Zhou J. Platelet-derived growth factor-B (PDGF-B) induced by hypoxia promotes the survival of pulmonary arterial endothelial cells through the PI3K/Akt/Stat3 pathway. *Cell Physiol Biochem* 2015: 35(2): 441-451.
39. Kaplan-Albuquerque N, Garat C, Desseva C, Jones PL, Nemenoff RA. Platelet-derived growth factor-BB-mediated activation of Akt suppresses smooth muscle-specific gene expression through inhibition of mitogen-activated protein kinase and redistribution of serum response factor. *J Biol Chem* 2003: 278(41): 39830-39838.
40. Urbich C, Knau A, Fichtlscherer S, Walter DH, Bruhl T, Potente M, Hofmann WK, de Vos S, Zeiher AM, Dimmeler S. FOXO-dependent expression of the proapoptotic protein Bim: pivotal role for apoptosis signaling in endothelial progenitor cells. *FASEB J* 2005: 19(8): 974-976.
41. Ackerman KG, Herron BJ, Vargas SO, Huang H, Tevosian SG, Kochilas L, Rao C, Pober BR, Babiuk RP, Epstein JA, Greer JJ, Beier DR. Fog2 is required for normal diaphragm and lung development in mice and humans. *PLoS Genet* 2005: 1(1): 58-65.
42. Ackerman KG, Wang J, Luo L, Fujiwara Y, Orkin SH, Beier DR. Gata4 is necessary for normal pulmonary lobar development. *Am J Respir Cell Mol Biol* 2007: 36(4): 391-397.
43. Bhatt AJ, Amin SB, Chess PR, Watkins RH, Maniscalco WM. Expression of vascular endothelial growth factor and Flk-1 in developing and glucocorticoid-treated mouse lung. *Pediatr Res* 2000: 47(5): 606-613.
44. Kunig AM, Balasubramaniam V, Markham NE, Morgan D, Montgomery G, Grover TR, Abman SH. Recombinant human VEGF treatment enhances alveolarization after hyperoxic lung injury in neonatal rats. *Am J Physiol Lung Cell Mol Physiol* 2005: 289(4): L529-535.

45. Bhandari V, Choo-Wing R, Lee CG, Zhu Z, Nedrelow JH, Chupp GL, Zhang X, Matthay MA, Ware LB, Homer RJ, Lee PJ, Geick A, de Fougerolles AR, Elias JA. Hyperoxia causes angiopoietin 2-mediated acute lung injury and necrotic cell death. *Nat Med* 2006: 12(11): 1286-1293.
46. Bhandari V, Elias JA. The role of angiopoietin 2 in hyperoxia-induced acute lung injury. *Cell Cycle* 2007: 6(9): 1049-1052.
47. Chen B. The miRNA-184 drives renal fibrosis by targeting HIF1AN in vitro and in vivo. *Int Urol Nephrol* 2019: 51(3): 543-550.
48. Pan L, Wang H, Jiang C, Li W, Chen Y, Ying G. Multiple MicroRNAs synergistically promote tolerance to epidermal growth factor receptor-targeted drugs in smoked lung cancer therapies. *J Cancer Res Ther* 2019: 15(4): 876-881.
49. Nagosa S, Leesch F, Putin D, Bhattacharya S, Altshuler A, Serror L, Amitai-Lange A, Nasser W, Aberdam E, Rouleau M, Tattikota SG, Poy MN, Aberdam D, Shalom-Feuerstein R. microRNA-184 Induces a Commitment Switch to Epidermal Differentiation. *Stem Cell Reports* 2017: 9(6): 1991-2004.
50. Najrana T, Mahadeo A, Abu-Eid R, Kreienberg E, Schulte V, Uzun A, Schorl C, Goldberg L, Quesenberry P, Sanchez-Esteban J. Mechanical stretch regulates the expression of specific miRNA in extracellular vesicles released from lung epithelial cells. *J Cell Physiol* 2020.

Figure Legends

Figure 1. miR-184 expression is upregulated in tracheal aspirates (TA), in lung tissues from human neonates with bronchopulmonary dysplasia (BPD) and in lungs of hyperoxia-induced murine model of experimental BPD. A) Increased miR-184 expression in cell pellets obtained from TA in the first postnatal week among neonates who subsequently did or did not develop BPD. Samples of TA from neonates who developed BPD (n=15) and did not develop BPD (n=10) were used for analysis, **p<0.01. **B)** miR-184 expression in whole lung tissues obtained from human neonates with BPD and term controls (n= 7 BPD patients and 5 age-matched controls, **p≤0.01. **C)** miR-184 levels in male and female human fetal lung Type II alveolar epithelial cells (TIIAECs) exposed to room air or RA (21% O_2) and hyperoxia (HYP, 60% O_2) at 6 and 24h (n=4 in each group, *p <0.05 and **p ≤0.01 for male TIIAECs and #p <0.05 and ##p ≤0.01 for female TIIAECs). **D, E)** miR-184-3p levels in lung tissues and in freshly isolated lung TIIAECs from room air (RA) and moderate hyperoxia (HYP, 60% O_2) exposed mice until postnatal days 4 (PN4), PN7 and in experimental BPD lungs where newborn mice were exposed to hyperoxia for first 4 days of life and then allowed to recover in RA till PN14. **F)** miR-184-3p levels in mice fetal lung TIIAECs exposed to RA and hyperoxia (HYP, 60% O_2) at 6, 12, 24 and 48h (n=4 in each group, *p <0.05, **p ≤0.01, ***p≤0.001 and ****p≤0.0001). **G,H)** miR-184 levels in mice and human (male and female) fetal lung ECs exposed to RA and hyperoxia (HYP, 60% O_2) at 6 and 24h. *In-vitro* experiments n= 4 were used and experiments were repeated 2 times (*p <0.05 for mice fetal lung ECs and for human male fetal lung ECs and #p ≤0.05 for human fetal female ECs). *In-vivo* experiments, n=7-9 mice were used in each group, *p<0.05, **p≤0.01 and ***p≤0.001. Data are expressed as mean ± SEM. For statistical analysis, student's unpaired *t-test* and one-way analysis of variance (ANOVA) followed by Tukey post hoc analysis were used.

Figure 2. miR-184-3p mimic exacerbates hyperoxia-induced lung injury and aberrant alveolarization in lungs. A) miR-184-3p expression in lungs of newborn mice treated with miR-184-3p mimic and exposed to room air (RA) or hyperoxia (n=7 in each group, *p<0.05 and **p<0.01). **B, C)** ELISA for IL6 and IL1β in lungs (n=6-8 in each group, *p<0.05 and ***p<0.001). **D)** Western blot analysis for IL6 and IL1β in lungs. Densitometric analysis shown below the immunoblots (n=4-8 in each group, *p<0.05, **p ≤0.01 and ***p ≤0.001). **E)** Western blot analysis for occludin and ZO-1 in lungs of RA and experimental bronchopulmonary dysplasia (BPD) mice treated with miR-184-3p mimic. Densitometric analysis is shown on the right of the immunoblots (n=4-6 in each group, *p<0.05 and **p<0.01). **F)** Immunofluorescence staining of ZO-1 in in fetal lung Type II alveolar epithelial cells (TIIAECs) transfected with miR-184-3p mimic (24h) and then exposed to hyperoxia (24h). Immunofluorescence intensities analysis shown to the right of images (n=3 in each group, *p <0.05, and ***p ≤0.001). Experiments were repeated twice. **G)** BAL fluid protein concentrations in RA and experimental BPD mice treated with miR-34a mimic (n=6-8 in each group, *p<0.05 and **p<0.01). **H)** Representative image of hematoxylin and eosin–stained lungs (n = 5 in each group). Scale bars: 100μm. Lung morphometric analyses measured as chord length **(I)**, radial alveolar counts **(J)**, septal thickness **(K)**, number of branches **(L)**, and number of junctions **(M)** in lungs of newborn mice treated with miR-184-3p mimic during hyperoxia or RA exposure. *p<0.05, **p ≤0.01, ***p ≤0.001 and ****p ≤0.0001. Data are expressed as mean ± SEM.

Figure 3. Inhibition of miR-184-3p alleviates hyperoxia-induced lung inflammation. A) Experimental plan for the newborn mice treated with miR-184-3p inhibitor (3μl in each nostril,

total dose of 20 μM) at postnatal (PN) day 1 (PN1) and PN3 during room air (RA) or hyperoxia exposure. **B, C)** Total and neutrophil cell counts in bronchoalveolar lavage (BAL) fluid from RA and experimental bronchopulmonary dysplasia (BPD) mice treated with miR-184-3p inhibitor (n =6-8 in each group, *p <0.05, **p ≤0.01 and ***p ≤0.001). **D)** Myeloperoxidase levels in lungs (n = 6-8 in each group, **p ≤0.01 and ***p ≤0.001). **E, F)** ELISA for IL6 and IL1β in lungs (n=8 in each group, *p <0.05, **p ≤0.01 and ***p ≤0.001). **G)** Western blot analysis for IL6 and IL1β in lungs RA and experimental BPD mice treated with miR-184-3p inhibitor. Densitometric analysis is shown on the right of the immunoblots (n=4-6 in each group, **p<0.01 and ***p<0.001). **H)** ELISA for IL6 and IL1β in fetal lung type II AECs (TIIAECs) exposed to room air (RA) or hyperoxia (HYP, 24h). Densitometric analysis shown on the right of the immunoblots (n=4 in each group, *p <0.05, and ***p ≤0.001). Experiments were repeated twice. Data are expressed as mean ± SEM.

Figure 4. Inhibition of miR-184-3p expression in lungs improves epithelial barrier function and pulmonary alveolarization in hyperoxia-induced bronchopulmonary dysplasia (BPD) lungs. A) Western blot analysis for occludin and ZO-1 in mice fetal lung Type II alveolar epithelial cells (TIIAECs) transfected with miR-184-3p inhibitor (24h) and then exposed to hyperoxia (24h). Densitometric analysis shown below the immunoblots (n=4 in each group, *p <0.05 and ***p ≤0.001). Experiments were repeated twice. **B)** Immunofluorescence staining of ZO-1 in in fetal lung Type II alveolar epithelial cells (TIIAECs) transfected with miR-184-3p inhibitor (24h) and then exposed to hyperoxia (HYP, 24h). Immunofluorescence intensities were shown on the right of the images (n=3 in each group, *p <0.05, and **p ≤0.01). Experiments were repeated twice. **C)** Western blot analysis for occludin and ZO-1 in lungs of room air (RA) and experimental BPD mice treated with miR-184-3p inhibitor. Densitometric analysis is shown on the right of the immunoblots (n=4 in each group, **p<0.01 and ***p<0.001). **D)** Total protein levels in bronchoalveolar lavage (BAL) fluid of RA and experimental BPD mice treated with miR-184-3p inhibitor. (n=7-8 in each group, p ≤0.01 and ***p ≤0.001). **E)** Representative image of hematoxylin and eosin–stained lungs (n = 5 in each group). Scale bars: 100μm. Lung morphometric analyses measured as chord length **(F)**, radial alveolar counts **(G)**, septal thickness **(H)**, number of branches **(I)** and number of junctions **(J)** in lungs of newborn mice treated with miR-184-3p inhibitor and exposed to RA or hyperoxia. *p <0.05, **p ≤0.01 and ***p ≤0.001. Data are expressed as mean ± SEM.

Figure 5. miR-184-3p targets PDGF-β and Fog2. A) Western blot analysis for PDGF-β and Fog2 in lung tissues from human neonates with bronchopulmonary dysplasia (BPD) and term controls. Densitometric analysis shown on the right of the immunoblots (n=5 in term control and-7 in BPD group, **p ≤0.01). **B)** Fetal lung Type II alveolar epithelial cells (TIIAECs) were transfected with PDGFβ 3'UTR (right bar) or co-transfected along with miR184-3p (left bar). Both GLuc activity and an internal control SEAP activity were determined 48h after transfection. The ratio of GLuc was normalized to SEAP. There is a significant suppression of the target gene PDGFβ by miR184-3p in AECII. **p ≤0.01 and experiments were repeated twice. **C)** Western blot analysis for PDGF-β and Fog2 in mice fetal lung Type II alveolar epithelial cells (TIIAECs) transfected with miR-184-3p inhibitor (24h) and then exposed to hyperoxia (24h). Densitometric analysis shown on the right of the immunoblots (n=4 in each group, *p <0.05 and **p ≤0.01). Experiments were repeated twice. **D)** Western blot analysis for PDGF-β lungs in room air (RA) and experimental BPD mice treated with miR-184-3p inhibitor. Densitometric analysis is shown below the immunoblots (n=4-6 in each group, *p <0.05, **p ≤0.01 and ***p ≤0.001). **E)** Western blot analysis for p-AKT and AKT in fetal lung Type II alveolar epithelial cells (TIIAECs) transfected with miR-184-3p inhibitor (24h) and then exposed to room air (RA) or hyperoxia

(HYP, 24h). Densitometric analysis is shown on the right of the immunoblots (n=4 in each group, **p ≤0.01 and ***p ≤0.001). Experiments were repeated twice. **F)** Western blot analysis for p-AKT and AKT in lungs of RA and experimental BPD mice treated with miR-184-3p inhibitor. Densitometric analysis is shown on the right of the immunoblots (n=6-8 in each group, ***p ≤0.001). **G)** Western blot analysis for PDGF-β and p-AKT in TIIAECs transfected with siRNA-PDGF-β (24h) and then exposed to room air (RA) or hyperoxia (HYP, 24h). Densitometric analyses were shown right to immunoblots (n=4 in each group, **p ≤0.01 and ***p ≤0.001). Experiments were repeated twice. Data are expressed as mean ± SEM.

Figure 6. miR-184-3p inhibition attenuates cell death by phosphorylation of Foxo3/Bcl2 mediated through AKT and PDGF signaling in hyperoxia. A) Western blot analysis for Foxo1 and Foxo3 translocation from the nucleus to cytosol fraction in lungs of room air (RA) and experimental bronchopulmonary dysplasia (BPD) mice treated with miR-184-3p inhibitor. Densitometric analysis is shown on the right of the immunoblots (n=4 in each group, *p <0.05, **p ≤0.01). **B)** Western blot analysis for Bax, Bcl_2 and cleaved caspase3 in lungs of RA and experimental BPD mice treated with miR-184-3p inhibitor. Densitometric analysis shown to the right of the immunoblots (n=4-6 in each group, *p <0.05, **p ≤0.01 and ***p ≤0.001). **C)** Western blot analysis for Bax, Bcl_2 and cleaved caspase3 in fetal lung Type II alveolar epithelial cells (TIIAECs) treated with miR-184-3p inhibitor (24h) and then exposed to hyperoxia (24h). Densitometric analysis shown to the right of the immunoblots (n=4 in each group, *p <0.05, **p ≤0.01 and ***p ≤0.001). Experiments were repeated twice. **D)** Representative figure of TUNEL staining (green color) of apoptotic cells in lungs of room air (RA) and experimental BPD mice treated with miR-184-3p inhibitor. (n = 5 in each group, **p ≤0.01 and ***p ≤0.001). **E)** Representative image of Ki67 staining (red) in lungs of RA and experimental BPD mice treated with miR-184-3p inhibitor. Scale bars: 100μm. Data are expressed as mean ± SEM.

Figure 7. Enhanced pulmonary alveolarization and vascularization by miR-184-3p inhibition are associated with improved lung mechanics in hyperoxia-induced bronchopulmonary dysplasia (BPD). A) Western blot analysis for VEGF-A, Ang1 and Ang2 in human fetal lung microvascular endothelial cells (ECs) transfected with miR-184-3p inhibitor (24h) and then exposed to hyperoxia (24h). Densitometric analysis shown below the immunoblots (n=4 in each group, *p <0.05, **p ≤0.01 and ***p ≤0.001). Experiments were repeated twice. **B)** Western blot analysis for VEGF-A, Ang1, and Ang2 in lungs of room air (RA) and experimental BPD mice treated with miR-184-3p inhibitor. Densitometric analysis shown below the immunoblots (n=4-6 in each group, *p <0.05, **p ≤0.01 and ***p ≤0.001). **C)** Representative image of von Willebrand Factor (vWF) staining in lungs of RA and experimental BPD mice treated with miR-184-3p inhibitor. Quantitative evaluations of vWF fluorescence staining of at least 6 fields of view of 3 independent experiments (n = 5 in each group, *p <0.05 and **p ≤0.01, Scale bars: 50μm.). Additonal images of vWF staining are shown in **Supplementary Figure 11**. **D-F)** Lung mechanics parameters measured by Flexivent (Scireq); lung compliance (Crs, n=7-8 in each group, **p ≤0.01 and ***p ≤0.001), Lung resistance (Rrs, n=7-8 in each group, *p <0.05 and **p ≤0.01) and lung elastance (Ers, n=7-8 in each group, *p <0.05 and **p ≤0.01) in lungs of room air (RA) and experimental BPD mice treated with miR-184-3p inhibitor. **G)** Schematic illustration of the proposed sequence of events in hyperoxia-induced BPD development mediated by upregulated miR-184-3p targeting Pdgf-β/Akt/Foxo3, Foxo1/Bax, Bcl2 signaling leading to impaired pulmonary alveolarization and Fog2/Vegf-A/Angiopoietin-1/2 pathway leading to deregulated angiogenesis in BPD lungs.

Figure 1

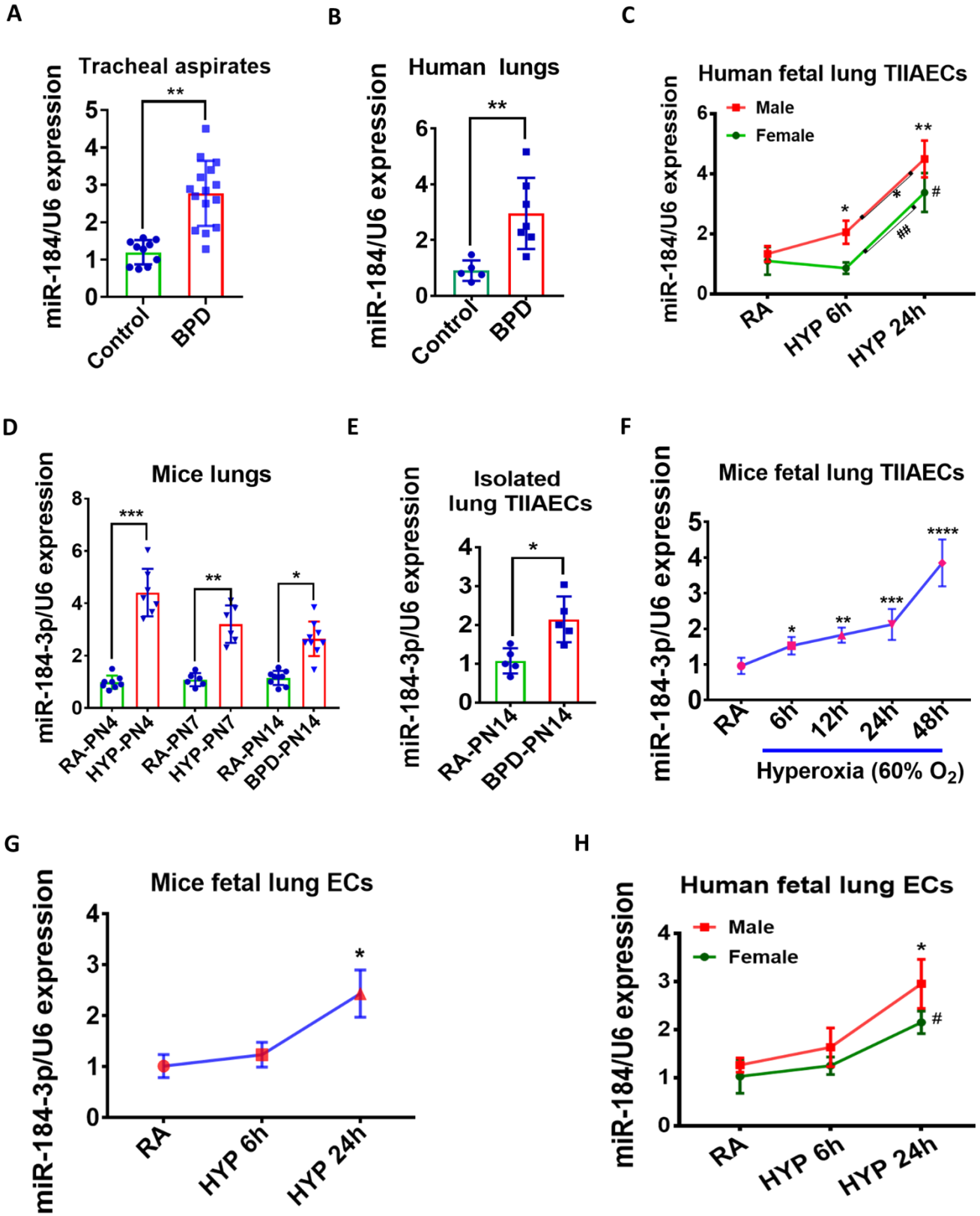
A
Tracheal aspirates
miR-184/U6 expression
Control
BPD
B
Human lungs
miR-184/U6 expression
Control
BPD
C
Human fetal lung TIIAECs
Male
Female
miR-184/U6 expression
RA
HYP 6h
HYP 24h
D
Mice lungs
miR-184-3p/U6 expression
RA-PN4
HYP-PN4
RA-PN7
HYP-PN7
RA-PN14
BPD-PN14
E
Isolated lung TIIAECs
miR-184-3p/U6 expression
RA-PN14
BPD-PN14
F
Mice fetal lung TIIAECs
miR-184-3p/U6 expression
RA
6h
12h
24h
48h
Hyperoxia (60% O2)
G
Mice fetal lung ECs
miR-184-3p/U6 expression
RA
HYP 6h
HYP 24h
H
Human fetal lung ECs
Male
Female
miR-184/U6 expression
RA
HYP 6h
HYP 24h

Figure 2

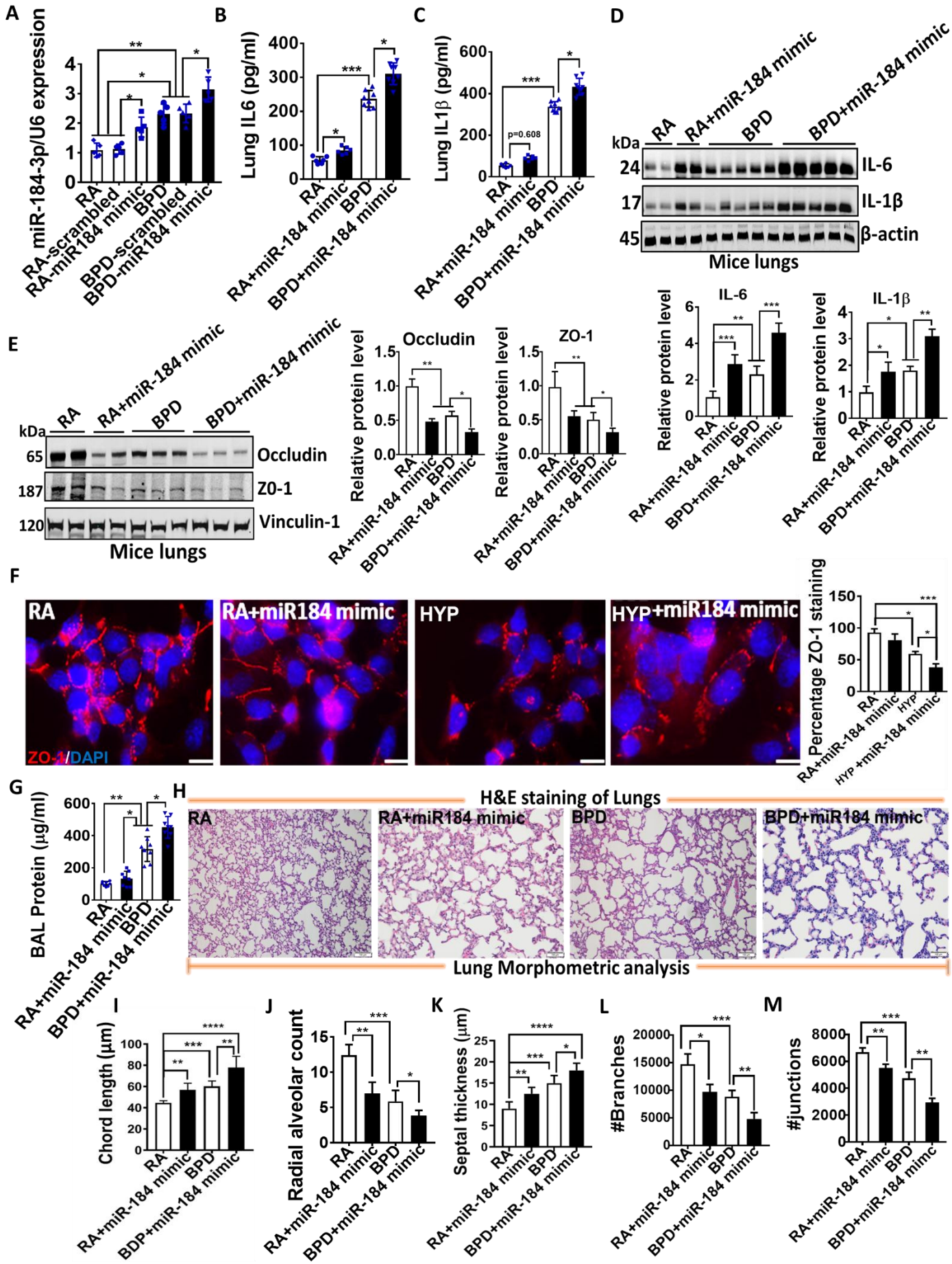
A
miR-184-3p/U6 expression
RA
RA-scrambled
RA-miR184 mimic
BPD
BPD-scrambled
BPD-miR184 mimic
B
Lung IL6 (pg/ml)
RA
RA+miR-184 mimic
BPD
BPD+miR-184 mimic
C
Lung IL1β (pg/ml)
p=0.608
D
kDa
IL-6
IL-1β
β-actin
Mice lungs
E
Occludin
ZO-1
Vinculin-1
Relative protein level
F
RA
RA+miR184 mimic
HYP
HYP+miR184 mimic
ZO-1/DAPI
Percentage ZO-1 staining
G
BAL Protein (μg/ml)
H
H&E staining of Lungs
Lung Morphometric analysis
I
Chord length (μm)
J
Radial alveolar count
K
Septal thickness (μm)
L
#Branches
M
#junctions

Figure 3

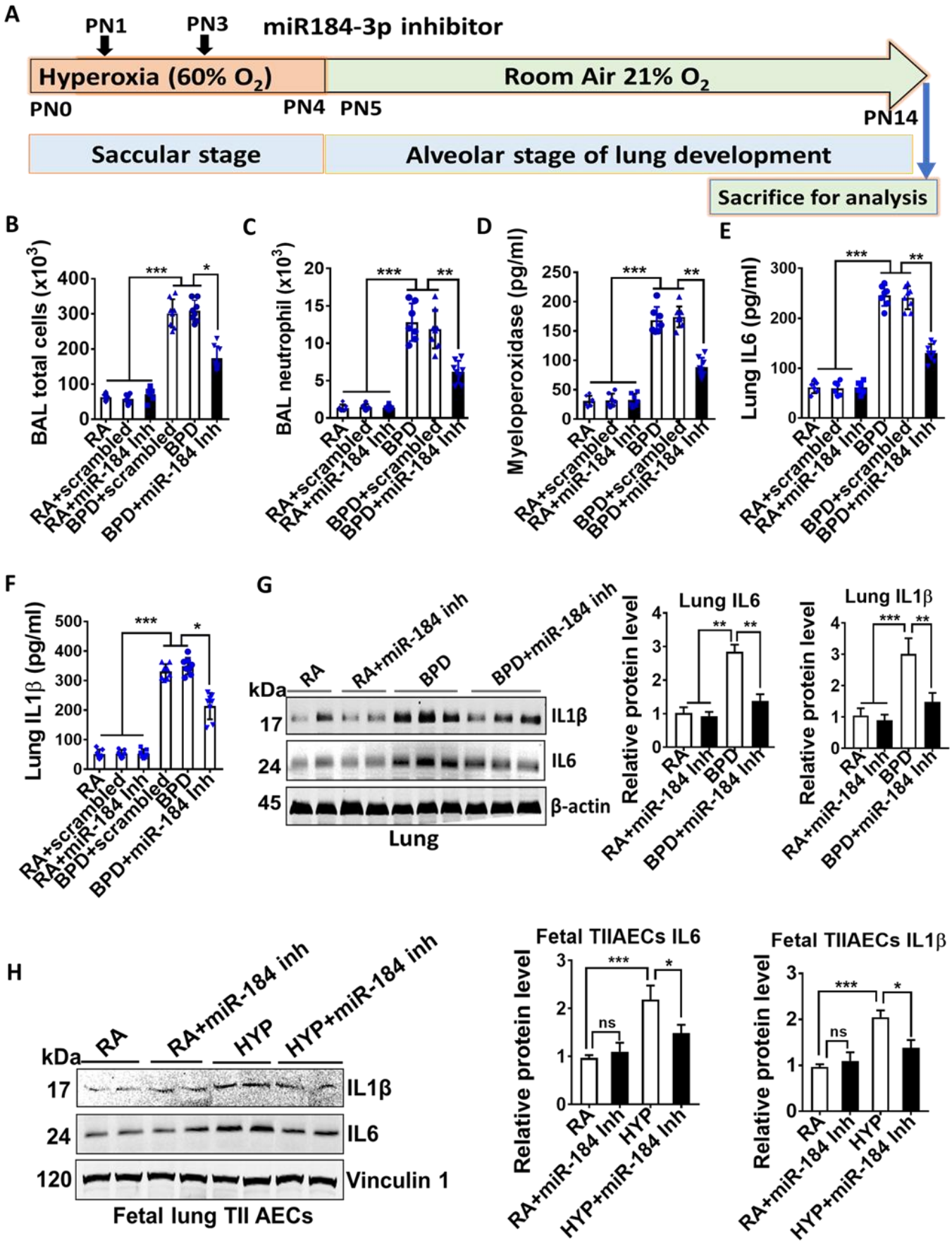
A
PN1
PN3
miR184-3p inhibitor
Hyperoxia (60% O2)
Room Air 21% O2
PN0
PN4
PN5
PN14
Saccular stage
Alveolar stage of lung development
Sacrifice for analysis
B
BAL total cells (x10^3)
C
BAL neutrophil (x10^3)
D
Myeloperoxidase (pg/ml)
E
Lung IL6 (pg/ml)
F
Lung IL1β (pg/ml)
RA
RA+scrambled
RA+miR-184 Inh
BPD
BPD+scrambled
BPD+miR-184 Inh
G
kDa
RA
RA+miR-184 inh
BPD
BPD+miR-184 inh
17
IL1β
24
IL6
45
β-actin
Lung
Lung IL6
Lung IL1β
Relative protein level
H
HYP
HYP+miR-184 inh
120
Vinculin 1
Fetal lung TII AECs
Fetal TIIAECs IL6
Fetal TIIAECs IL1β
ns

Figure 4

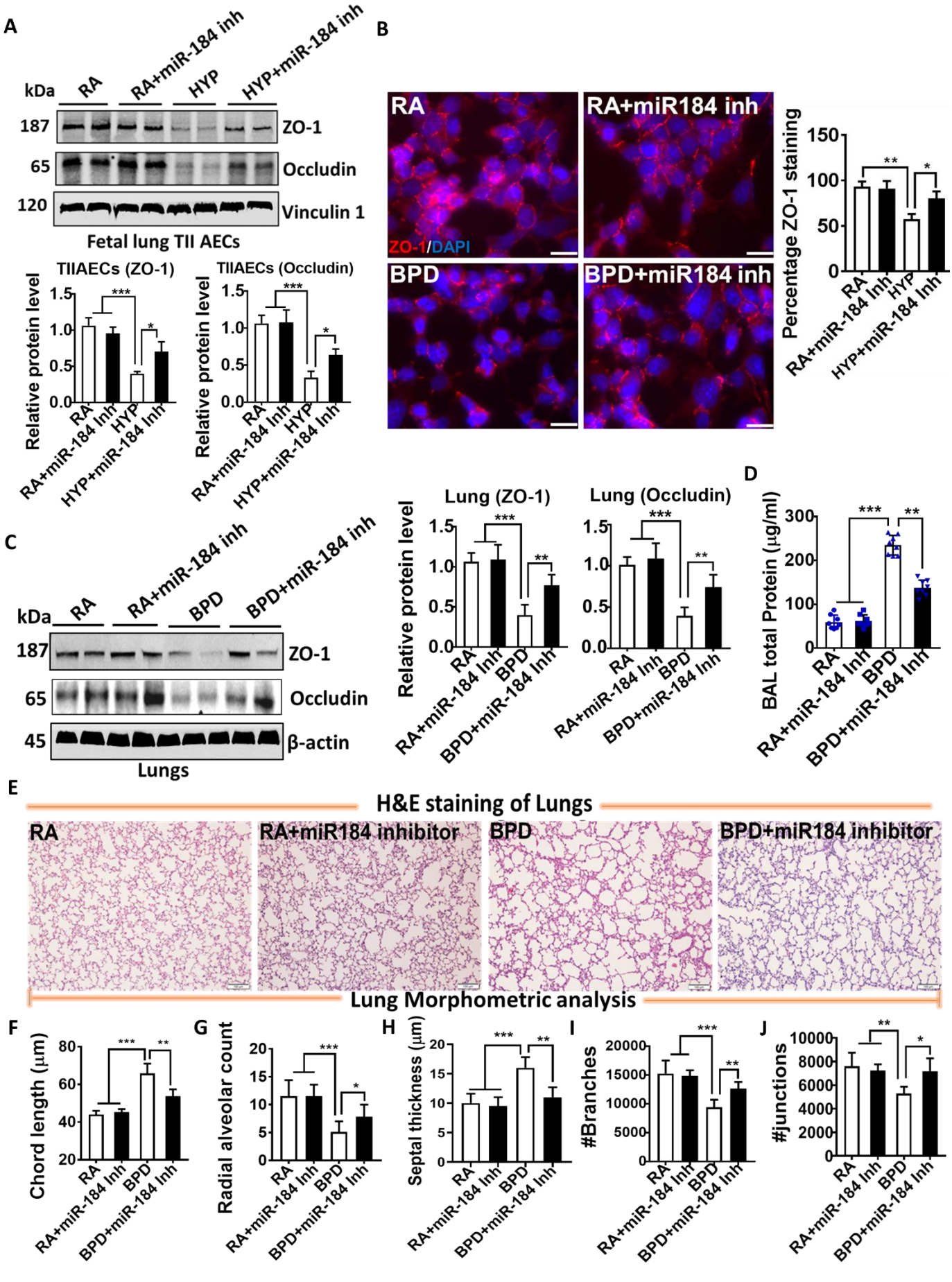
A
kDa
RA
RA+miR-184 inh
HYP
HYP+miR-184 inh
187
ZO-1
65
Occludin
120
Vinculin 1
Fetal lung TII AECs
TIIAECs (ZO-1)
TIIAECs (Occludin)
Relative protein level
RA
RA+miR-184 Inh
HYP
HYP+miR-184 Inh
B
RA
RA+miR184 inh
BPD
BPD+miR184 inh
ZO-1/DAPI
Percentage ZO-1 staining
C
BPD
BPD+miR-184 inh
45
β-actin
Lungs
Lung (ZO-1)
Lung (Occludin)
D
BAL total Protein (μg/ml)
E
H&E staining of Lungs
RA+miR184 inhibitor
BPD+miR184 inhibitor
Lung Morphometric analysis
F
Chord length (μm)
G
Radial alveolar count
H
Septal thickness (μm)
I
#Branches
J
#junctions

Figure 5

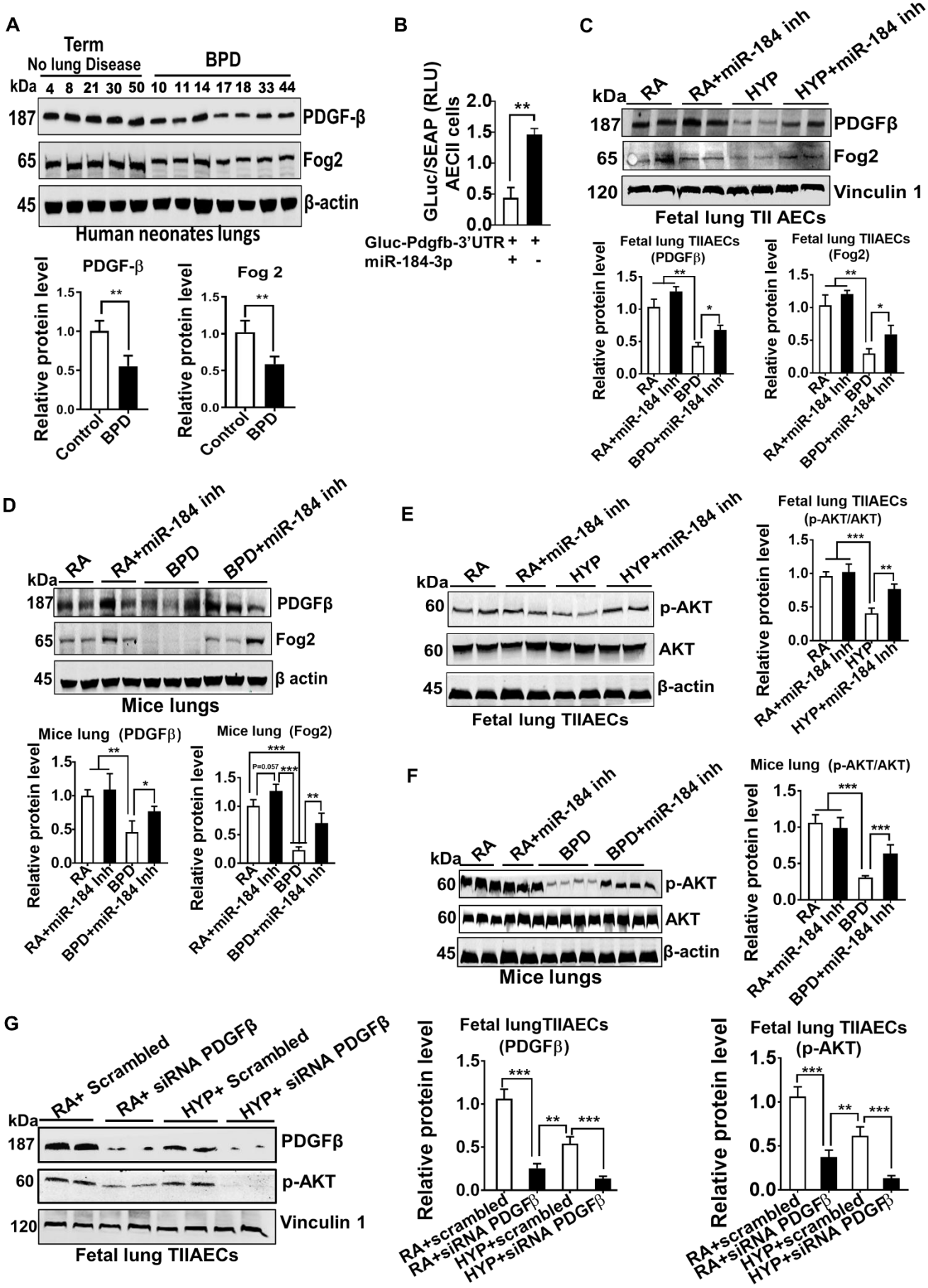
A
Term
No lung Disease
BPD
kDa 4 8 21 30 50 10 11 14 17 18 33 44
187
PDGF-β
65
Fog2
45
β-actin
Human neonates lungs
PDGF-β
Fog 2
Relative protein level
Control
BPD
B
GLuc/SEAP (RLU)
AECII cells
Gluc-Pdgfb-3'UTR + +
miR-184-3p + -
C
RA
RA+miR-184 inh
HYP
HYP+miR-184 inh
PDGFβ
Fog2
120
Vinculin 1
Fetal lung TII AECs
Fetal lung TIIAECs (PDGFβ)
Fetal lung TIIAECs (Fog2)
RA+miR-184 Inh
BPD
BPD+miR-184 Inh
D
BPD+miR-184 inh
Mice lungs
Mice lung (PDGFβ)
Mice lung (Fog2)
P=0.057
E
p-AKT
AKT
Fetal lung TIIAECs
Fetal lung TIIAECs (p-AKT/AKT)
F
Mice lung (p-AKT/AKT)
G
RA+ Scrambled
RA+ siRNA PDGFβ
HYP+ Scrambled
HYP+ siRNA PDGFβ
Fetal lung TIIAECs
Fetal lungTIIAECs (PDGFβ)
Fetal lung TIIAECs (p-AKT)
RA+scrambled
RA+siRNA PDGFβ
HYP+scrambled
HYP+siRNA PDGFβ

Figure 6

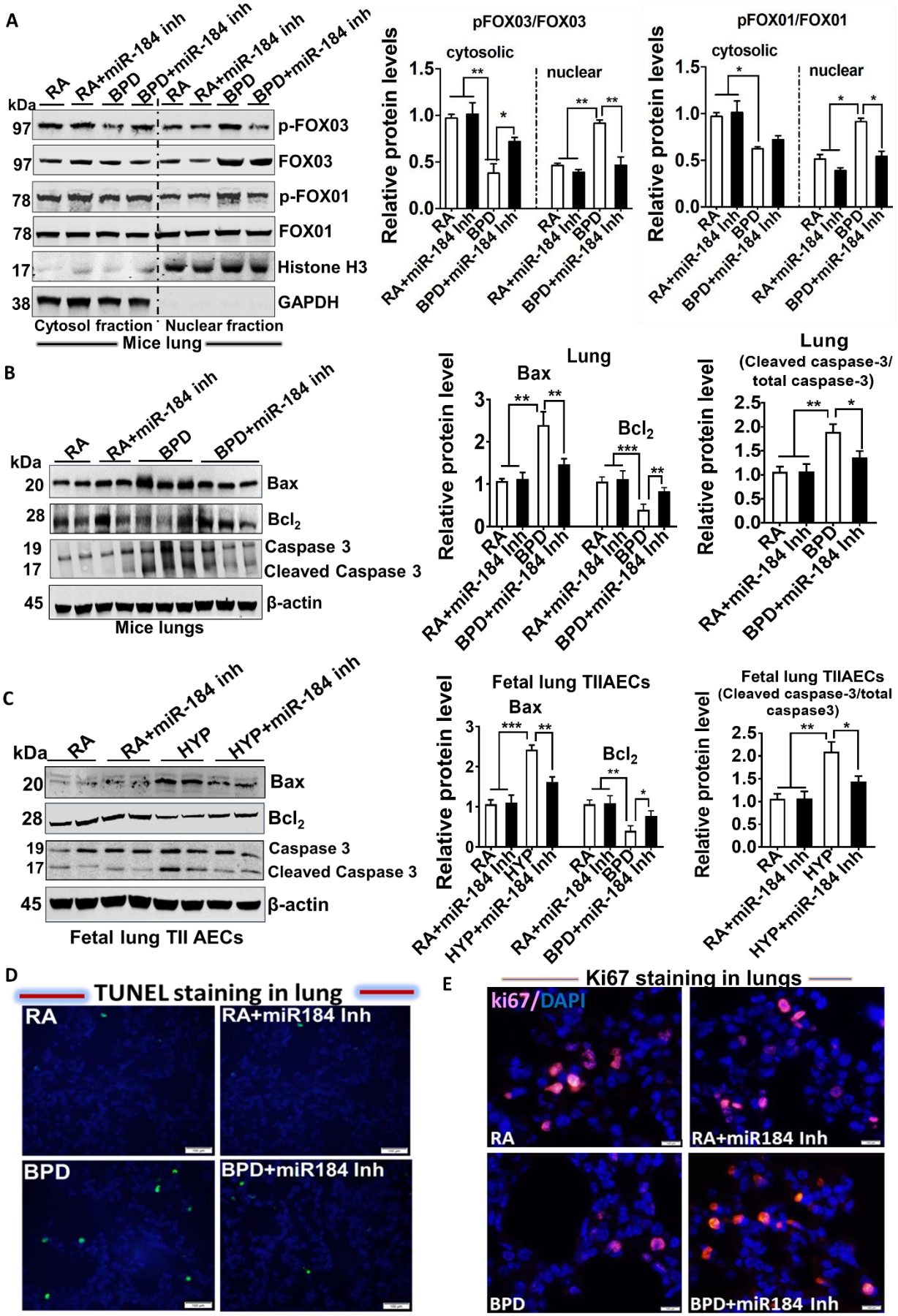
A
RA
RA+miR-184 inh
BPD
BPD+miR-184 inh
kDa
97
p-FOX03
97
FOX03
78
p-FOX01
78
FOX01
17
Histone H3
38
GAPDH
Cytosol fraction
Nuclear fraction
Mice lung
pFOX03/FOX03
cytosolic
nuclear
Relative protein levels
pFOX01/FOX01
B
Bax
Bcl2
Caspase 3
Cleaved Caspase 3
β-actin
Mice lungs
Lung
Lung
(Cleaved caspase-3/
total caspase-3)
C
HYP
HYP+miR-184 inh
Fetal lung TII AECs
Fetal lung TIIAECs
Fetal lung TIIAECs
(Cleaved caspase-3/total
caspase3)
D
TUNEL staining in lung
RA
RA+miR184 Inh
BPD
BPD+miR184 Inh
E
Ki67 staining in lungs
ki67/DAPI

Figure 7

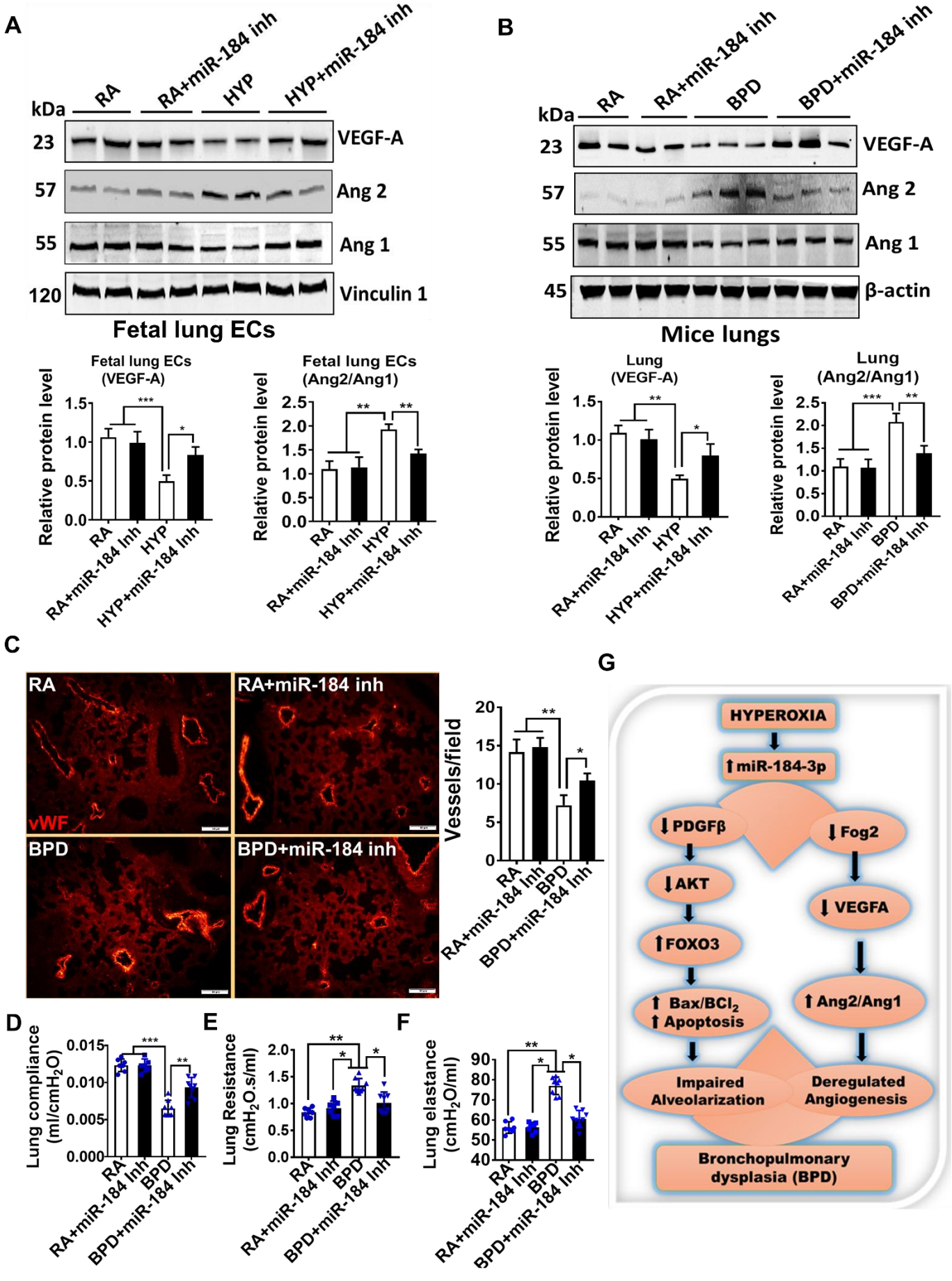
A
RA
RA+miR-184 inh
HYP
HYP+miR-184 inh
kDa
23
VEGF-A
57
Ang 2
55
Ang 1
120
Vinculin 1
Fetal lung ECs
Fetal lung ECs (VEGF-A)
Relative protein level
Fetal lung ECs (Ang2/Ang1)
B
BPD
BPD+miR-184 inh
45
β-actin
Mice lungs
Lung (VEGF-A)
Lung (Ang2/Ang1)
C
vWF
Vessels/field
D
Lung compliance (ml/cmH2O)
E
Lung Resistance (cmH2O.s/ml)
F
Lung elastance (cmH2O/ml)
G
HYPEROXIA
↑miR-184-3p
↓PDGFβ
↓Fog2
↓AKT
↓VEGFA
↑FOXO3
↑ Bax/BCl2
↑ Apoptosis
↑Ang2/Ang1
Impaired Alveolarization
Deregulated Angiogenesis
Bronchopulmonary dysplasia (BPD)

Online Information

miR-184 mediates hyperoxia-induced injury by targeting cell death and angiogenesis signaling pathways in the developing lung

Dilip Shah, PhD[1#], Karmyodh Sandhu, MS[1], Pragnya Das, PhD[1#], Zubair H. Aghai[2], Sture Andersson, MD, PhD[3], Gloria Pryhuber, MD[4], and Vineet Bhandari, MD, DM[1*#]

[1]Section of Neonatal-Perinatal Medicine, Department of Pediatrics, Drexel University College of Medicine, Philadelphia, PA, USA

[2]Division of Neonatology, Department of Pediatrics, Thomas Jefferson University Hospital, Philadelphia, PA, 19107, USA.

[3]Children's Hospital, University of Helsinki and Helsinki University Hospital, Helsinki, Finland

[4]Department of Pediatrics, University of Rochester School of Medicine and Dentistry, Rochester, NY, USA

***Corresponding Author**

[#]**Current Affiliation**: Neonatology Research Laboratory (Room #206), Education and Research Building, Cooper University Hospital, Camden, NJ

Methods:

Murine model of hyperoxia-induced experimental BPD

The hyperoxia-induced murine model of experimental BPD is well established in our laboratory (1-3) where newborn mouse pups (within 12h of birth) of both sexes were exposed to moderate hyperoxia [60% oxygen (2, 4)] from postnatal day 0 (PN0; saccular stage of mouse lung development) to PN 4 (initiation of alveolar stage of mouse lung development) and then allowed to recover in room air (21% oxygen) till PN14 (alveolar stage), as previously described (1-3). We have selected to expose newborn mice from PN0 - PN4 because the mice lungs are at the saccular stage of lung development, which is equivalent to ~26 – 36 weeks gestational age in human neonates; this is the gestational age of human neonates most at-risk for developing BPD. Also, we and others have reported that moderate hyperoxia (60% O_2 concentration)-induced injury to the mice lung at the saccular stage (PN0-PN4) of lung development mimics the human BPD pulmonary phenotype with alveolar size and lung compliance increased, and airway resistance, airway elastance, tissue elastance, and tissue damping decreased. (3, 5-7). This level of O_2 is also clinically relevant to neonates managed in the neonatal intensive care units (NICUs).

The hyperoxia environment was established by utilizing a Plexiglas chamber (55 × 40 × 50 cm) attached to a source of oxygen. Oxygen levels were continuously monitored with a ProOX 360 (BioSpherix, NY), nursing dams were rotated between exposure groups (room air and hyperoxia) every 24h to prevent oxygen toxicity to the dams and to mitigate nutritional effects between the experimental groups. The control group, room air-exposed mice were housed in standard cages. At the end of experimental time points, these mice were euthanized according to the IACUC approved protocol by the injection (i.p.) of overdose of xylazine (100mg/kg)/ketamine (10mg/kg) mixture (0.1ml per 10 gm of body weight of mice) and BAL fluid and lung tissues were harvested for further analysis.

miR-184-3p mimic and inhibitor experiments

Syn-mmu-miR-184-3p miScript miRNA mimic (5 'UGGACGGAGAACUGAUAAGGGU, Catalog no. MSY0000213) and anti-mmu-miR-184-3p miScript miRNA inhibitor (5 'UGGACGGAGAACUGAUAAGGGU, Catalog no. MIN0000213), anti-hsa-miR-184 miScript miRNA Inhibitor (5 'UGGACGGAGAACUGAUAAGGGU, Catalog no. MIMAT0000454) were procured from Qiagen (Frederick, MD) and reconstituted to 20 μM, following manufacturer's instructions. Briefly, newborn pups were exposed to hyperoxia or room air immediately after birth and three microliters of miR-184-3p mimic or inhibitor were administered intranasally to each nostril on PN1 and PN3 as described previously (3).

Analysis of bronchoalveolar lavage (BAL) Fluid

BAL was performed by cannulating the trachea with a small-caliber needle. Two volumes of 300μl of cold 1X phosphate-buffered saline (PBS) were instilled, gently aspirated, and pooled. Total cell counts in BAL fluid were determined using the TC20 automated cell counter (Bio-Rad Laboratories, Inc., Hercules, CA). The differential cell counts were performed on cells cytocentrifuged onto glass slides (Fisher Scientific) stained with the Hema 3 Staining System (Fisher Scientific, Kalamazoo, MI) and cell differential was tabulated using light microscopy. Total protein concentration in the BAL fluid was measured using the Pierce^{TM} BCA assay kit (Fisher Scientific Co, Houston, TX), as previously described (2).

***In-vitro* overexpression and inhibition of miR-184-3p**

Fetal mice lung TIIAECs (MPAEpiC) were transfected with the mixtures of HiPerFect reagent (Qiagen, Catalog no. 301704) and Syn-mmu-miR-184a-3p miScript miRNA Mimic (5 'UGGACGGAGAACUGAUAAGGGU, working dilution10nM, Catalog no MSY0000213, Qiagen), Anti-mmu-miR-184-3p miScript miRNA Inhibitor (5 'UGGACGGAGAACUGAUAAGGGU, working dilution 20nM, Catalog no. MIN0000213, Qiagen) or scrambled mimic (10nM) as negative control (Qiagen, SI03650318) were performed in Opti-mem^{TM} for 15 min prior to transfection to allow the

miR-184-3p mimic- or scrambled mimic-complexes to form and then added to fetal lung TIIAECs and ECs grown in 6 well plates. After 24h, transfected cells were used for experiments. Similar procedures were followed for transfection of human fetal lung TIIAECs using anti-hsa-miR-184 miScript miRNA inhibitor (5 'UGGACGGAGAACUGAUAAGGGU, Catalog no. MIN0000454, Qiagen) and miScript inhibitor negative control (Catalog no. 1027271) as described previously (8).

Quantitative Real-time PCR analysis

For miR-184 analysis, total RNA was extracted using the Qiagen miRNeasy Kit (Qiagen, Frederick, MD) and one µg of total RNA was used for cDNA preparation using miScript II RT Kit (Qiagen). Real-time PCR was performed in a 20-µl volume using QuantiTect SYBR Green PCR Kit (Qiagen) and miScript specific primers and RNU6 as the endogenous control were used. The StepOnePlus platform (Applied Biosystems) was used for all PCR, done in triplicate. Changes in expression were calculated by the change in threshold (ΔΔCT) method with RNU6 as the endogenous control for miRNA analysis. The miScript primers (Qiagen) IDs are mouse MIMAT0000213: 5'UGGACGGAGAACUGAUAAGGGU (Mm-miR-184-3p, Catalog no. MS00001729), MIMAT0022690: 5'CCUUAUCACUUUUCCAGCCAGC (Mm-miR-184-5p, Catalog no. MS00042546) and human MIMAT0000454: 5'UGGACGGAGAACUGAUAAGGGU (Hs-miR-184, Catalog no. MS00003640).

Cellular fractionation

Nuclear and cytoplasmic fractions were prepared from whole lungs of RA and experimental BPD mice using the Nuclear Extract Kit as per manufacturer's instructions with modifications (Active Motif). Briefly, after collecting the cytoplasmic fraction, nuclear pellets were re-suspended in 50µl complete lysis buffer and incubated for 30 minutes on ice on a rocking platform. Samples were vortexed for 30 seconds and centrifuged for 10 minutes at 14,000 × g and the nuclear fraction (as supernatants) were collected for protein analysis.

Western Blotting

Lung Type II AECs pellets or whole lung tissues were homogenized in ice-cold RIPA buffer containing protease inhibitors (Roche Complete mini) and phosphatase inhibitors (Roche Complete mini) as previously described (9). Cell lysate and lung homogenate were centrifuged (14,000 × g) at 4 °C for 15 min and the supernatant was collected for further analysis. Thirty micrograms of protein were loaded onto each well, separated on 10% SDS-polyacrylamide gel and then transferred onto a nitrocellulose membrane (Bio-Rad) using a Bio-Rad Mini-Blot transfer apparatus. Immunoblotting was performed at 4°C overnight using primary antibodies directed against AKT (Dilution 1/1000, Catalog no. 4685, Cell Signaling, Danvers, MA), p-AKT (Dilution 1/1000, Catalog no. 4058, Cell Signaling, Danvers, MA), angiopoietin-1 (Dilution 1/500, Catalog no. AB10516, Sigma-Aldrich, MO), angiopoietin-2 (Dilution 1/500, Catalog no. 176002, Sigma-Aldrich, MO), p-FOXO3 (Dilution 1/500, Catalog no. 9466, Cell Signaling, Danvers, MA), FOXO3 (Dilution 1/500, Catalog no. 2497, Cell Signaling, Danvers, MA), p-FOXO1 (Dilution 1/1000, Catalog no. 2486, Cell Signaling, Danvers, MA), FOXO1 (Dilution 1/1000, Catalog no. 2880, Cell Signaling, Danvers, MA), ZO-1 (Dilution 1/1000 for WB, 1/100 for immunofluorescence, Catalog no. 61-7300, ThemoFisher Scientific), Occludin (Dilution 1/1000, Catalog no. 5446, Cell Signaling, Danvers, MA), IL1β (Dilution 1/1000, Catalog no. 12242, Cell Signaling, Danvers, MA), IL6 (Dilution 1/1000, Catalog no. 12912, Cell Signaling, Danvers, MA), cleaved caspase-3 (Dilution 1/1000, Catalog no. 9664, Cell Signaling, Danvers, MA), and β-actin (Dilution 1/1000, Catalog no. 8457, Cell Signaling, Danvers, MA), vinculin-1 (Dilution 1/1000, Catalog no. 13901, Cell Signaling, Danvers, MA). Membranes were then incubated with a 1:10,000 dilution of a secondary antibodies (IRDye 800CW Goat anti-Mouse IgG (P/N 926-32210 and IRDye 800CW Goat anti-Mouse IgG (P/N 926-32211, Li-Cor Biosciences, Lincoln, NE) at room temperature for 1h. Immunoblots were visualized using the Odyssey infrared imaging system (Li-Cor Biosciences, Lincoln, NE). The band intensity on the western blots was analyzed using the Image J software (Version 1.6, National Institutes of Health, MD).

Immunohistochemistry in human and mice neonatal lungs

Collection and processing of the human lung samples from premature infants having the diagnoses of BPD were approved by the National Supervisory Authority for Welfare and Health in Finland and the University of Rochester Institutional Review Board. Selected clinical details have been shown in **Supplemental Tables E2 and E3**. Sections were stained with primary antibody against Pdgf-β (1/100 dilution, Abcam; Catalog no. ab23914, Cambridge, MA) and goat anti-rabbit IgG secondary antibody, Rhodamine conjugate (1/200 dilution, Catalog no. 31670, Invitrogen). Similarly, mice lung sections were stained with primary antibody against Fog2 (1/100 dilution, Abcam; Catalog no. ab23914, Cambridge, MA) and goat anti-rabbit IgG secondary antibody, Rhodamine conjugate (1/200 dilution, Catalog no. 31670, Invitrogen). Four to five random images per lung were taken using a fluorescence microscope (Olympus Co., Tokyo, Japan).

Terminal deoxynucleotidy1 transferase-mediated dUTP nick end-labeling (TUNEL) assay

Apoptosis in lungs tissues were confirmed by TUNEL assay using the fluorescence based TUNEL Kit (In Situ Cell Death Detection Kit, Roche Diagnostics) according to the manufacturer's instructions. In brief, de-paraffinized lung tissue sections were permeabilized using 0.3% Triton-X 100, blocked with 1% BSA and then incubated with TUNEL reaction mixture (1 part of enzyme solution and 9 parts of label solution) for 1h at 37^{o}C in dark. Slides were washed with PBS, mounted with Vectashield mounting solution with DAPI (Catalog no. H-1800-10, Vector Laboratories) and visualized with a fluorescent microscope using an exciting wavelength of 460-490 nm. Percentage TUNEL positive cells were expressed as total number of green positive cells/total number of DAPI positive cells.

Analysis of cell proliferation

Cell proliferation in the lungs of RA and experimental BPD mice treated with miR-184-inhibitor was studied by co-immunofluorescent detection of the proliferation marker Ki-67 (Red, Texas Red) (2).The Ki-67 labeling index of air-exchanging parenchyma was determined by manually counting the number of Ki-67–positive nuclei relative to the total number of nuclei (proliferative index) within

distal lung parenchyma. For each lung, at least 10 randomly selected fields per slide were evaluated (magnification X40).

von Willebrand factor (VWF)

Pulmonary vessel density was determined based on immunofluorescence staining of vWF, an endothelial cell-specific marker, in the lung sections as described previously (2). In brief, de-paraffinized lung sections (5µm) were incubated with CAS Block^{TM} solution (Catalog no. 008120, Life Technology) for one hour and then stained with primary antibody specific to vWF (1:100 dilution, Abcam; catalog no. ab6994, Cambridge, MA) diluted in antibody diluent (Catalog no. 003118, Invitrogen) for overnight. In the following morning, lung sections were stained with Alexa Fluor anti-mouse IgG for secondary fluorescent antibodies (1/100 dilution, Molecular Probes, Eugene, OR). For nuclear staining, sections were mounted with DAPI medium (Catalog no. H-1800-10, Vector Laboratories) and images were taken under the fluorescence microscope (Olympus, Tokyo, Japan) in a blinded manner. Microvascular density and quantitation were assessed in lung sections stained for vWF at a 200x magnification by counting the number of vessels per field as previously described (10, 11). This analysis was performed in a blinded manner of at least of 6 representative fields per experimental animal investigated. Single red-staining endothelial cells or clusters of endothelial cells, with or without a lumen, were counted as individual microvessels, and pulmonary vessels with a diameter of >100 µm were excluded from the analysis. Positive-stained cells were counted at five representative locations under high magnification using ImageJ software (National Institutes of Health) and the results were averaged.

Histological analysis

Mice were killed by an intraperitoneal (*i.p.*) injection with an overdose of xylazine/ketamine. The trachea was cannulated, and the lungs were fixed with 4% paraformaldehyde at 25 cm H_2O inflation pressure for 15 minutes. Trachea was tied off and lungs were dissected and fixed wholes lungs were fixed overnight in 4% paraformaldehyde and subsequently embedded in paraffin. Lung

tissues sections (5µm) and H&E staining were performed at the Department of Pathology Core Facility (DUCOM). Four to five random images from several transverse slices per lung lobe and five to six lungs per experimental group were characterized for measuring lung morphometric analysis.

Lung Morphometric analysis

Four to five random images per lung and six lungs per experimental group were characterized for measuring lung morphometric analysis (chord length and septal thickness) using ImageJ (1, 2). The alveolar size was estimated from the mean chord length of the airspace and radial alveolar counts (RAC) were done as described previously (1). Number of branches and junctions were calculated using AnalyzeSkeleton program from ImageJ software. This plugin tags all pixel/voxels in a skeleton image and then counts all its junctions, and branches.

Measurement of lung mechanics

Lung mechanics such as lung resistance, lung compliance, and tissue elastance were measured in anesthetized neonatal mice as previously described (12). In brief, before each mouse was connected to the flexiVent, the calibration signals were collected by applying a volume perturbation initially through a completely closed tracheal cannula and then opened to the atmosphere to estimate the flow resistance of the tracheal cannula and the elastance of air in the ventilator cylinder. To provide a constant volume history, a 6-second-deep inflation maneuver to 27 cmH_2O was performed twice prior to data collection. Mice were mechanically ventilated in a supine position at a respiratory rate of 150 breaths/min and at a tidal volume of 10ml/kg, with a pressure limit of 30 cmH_2O coupled to a constant positive expiratory end-pressure (PEEP) of 3 cmH_2O using the flexiVent (SCIREQ, Montreal, Canada) module FX1 ventilation set up.

Isolation of lung Type II AECs

Lung TIIAECs were isolated from murine lungs as per our earlier published method using MACS cell separation (Miltenyi Biotec, Spain) (13). Briefly, mice were anesthetized with a ketamine/xylazine mixture and the pulmonary vasculature was perfused with ice-cold saline. The trachea was cannulated with one inch 18G blunt tip syringe needles and the lungs were filled with 0.5 ml dispase (BD Bioscience, San Jose, CA) and then 0.2 ml of low melting agarose was infused into the airways via the trachea and lungs were placed in ice for 1 min to harden the agarose. Lungs were minced and transferred in 14-ml GentleMACS C tube containing 1-ml dispase for 6 minutes in water bath at 37°C. Tube was inserted in GentleMACS and run m_lung_1.01 program to gently mince lung for 8 seconds (14). Lung homogenates were filtered through 100 µm and 40 µm then lung cells were stained with CD45 microbeads (Miltenyi Biotec) for negative selection. Lung TIIAECs were purified by positive selection for the epithelial cell adhesion molecule (Ep-CAM) using magnetic labeling with streptavidin microbeads in MACS LS columns (Miltenyi Biotec). Cells pellets were homogenized in ice-cold RIPA buffer containing protease inhibitors (Roche Complete mini) and phosphatase inhibitors (Roche Complete mini), as previously described (9).

Lung cell lines and cell culture

C57BL/6 mouse fetal lung Type II AECs (MPAEpiC, Catalog No. C57-6053E), C57BL/6 mouse fetal pulmonary microvascular endothelial cells (MPMEC, C57-6011E) and complete medium were purchased from Cell Biologics (Chicago, IL). The human fetal lung alveolar epithelial cells (HPAEpiC, Catalog No. 3200, Lot # 27013 (Donor: 20 weeks gestation, female,) and Lot #27558 (Donor: 18 weeks gestation, male), microvascular endothelial cells (HPMEC, Catalog No. 3000) and respective complete medium were purchased from ScienCell Research Laboratories, Inc., Carlsbad, CA. MPAEpiC and MPMEC from Cell Biologics were isolated from lung tissue of pathogen-free laboratory mice at embryonic day 17. As per ScienCell (Carlsbad, CA) information, HPAEpiC were isolated from donor human lung tissue at gestation weeks 18-19. We have used HPAEpiC (lot #27013) obtained from female human lung tissue at gestation weeks 20 and HPAEpiC lot #27558 obtained from male human lung tissue at gestation weeks 18. Similarly,

HPMEC used in this study were isolated from the donor of human lung tissues (18-20 weeks of gestation age). Per ScienCell, the tissue is obtained from nonprofit tissue providers who strictly adhere to the guidelines for tissue collection and distribution according to established protocols in compliance with local, state, and federal laws and regulations governing the procurement and distribution of human tissue after informed consent. The details regarding the ethics for tissue collection from donors and the protocol have been described previously (15). Cells were maintained in 10-cm plastic dishes pre-coated with gelatin-based coating solution (for MPAEpiC and MPMEC), poly-L-lysine (for HPAEpiC) and fibronectin (for HPMEC) according to the instructions provided by Cell Biologics (Chicago, IL), and ScienCell (Carlsbad, CA). For some experiments, these cells were exposed to hyperoxia (60% O_2) and room air (21% O_2) for multiple time points. At specified time points, cell pellets and cell lysates were collected for analysis. These cells were used in experiments between the 4-6 passages and for each set of experiments the same passage of cells were used.

Cell transfection

Lung alveolar epithelial cells grown to 70% confluence were transfected with a smart pool of 3 target specific for mouse PDGF-b siRNA (Sc-39706, Santa Cruz Biotechnology, Inc) and control siRNA-A (Sc-37007, Santa Cruz Biotechnology, Inc) at a concentration of 100 nM using siRNA transfection reagent (Sc- 29528, Santa Cruz Biotechnology, Inc) according to the manufacturer's instructions and an earlier published method (16). Cells were transfected for 24 h in serum-free medium, followed by exposure to hyperoxia or room air for next 24h. After the experimental time point, transfected cells were used for experiments. A similar method was followed for knockdown of Fog2 in ECs using a smart pool of 3 target specific for mouse Fog2-siRNA (Sc-39706, Santa Cruz Biotechnology, Inc).

Luciferase assay

Both MLE12 (adult mouse lung epithelial cells) and AEC II (neonatal mouse lung epithelial Cells) were transfected with pEZX-MT05 target expression vector alone, which expresses Gaussia Luciferase (GLuc) under the control of SV40 promoter, along with a secreted alkaline phosphate (SEAP) driven reporter under the control of CMV promoter, cloned downstream of 3'UTR of Pdgfb in the same vector, or co-transfected with psi-AVE001-miR184-3p. Briefly, $2x10^5$ cells were plated on 24-wells plate and transfected with the above dual reporter plasmids to assess for the interaction of miR184-3p with its target Pdgfb for 48h, following which luminescence was detected using the dual luciferase reporter detection kit (GeneCopoeia, MD, USA) following the manufacturer's instructions, in a 96-well plate reader (BioTek Synergy), with an integration time set at 1sec. pEF1A-PG04 was used as a positive control. A similar procedure was followed for another target Fog2 for miR184-3p in lung ECs.

References:

1. Syed M, Das P, Pawar A, Aghai ZH, Kaskinen A, Zhuang ZW, Ambalavanan N, Pryhuber G, Andersson S, Bhandari V. Hyperoxia causes miR-34a-mediated injury via angiopoietin-1 in neonatal lungs. *Nat Commun* 2017; 8: 1173.
2. Syed MA, Shah D, Das P, Andersson S, Pryhuber G, Bhandari V. TREM-1 Attenuates RIPK3 Mediated Necroptosis in Hyperoxia Induced Lung Injury in Neonatal Mice. *Am J Respir Cell Mol Biol* 2018.
3. Leary S, Das P, Ponnalagu D, Singh H, Bhandari V. Genetic Strain and Sex Differences in a Hyperoxia-Induced Mouse Model of Varying Severity of Bronchopulmonary Dysplasia. *Am J Pathol* 2019; 189: 999-1014.
4. Buczynski BW, Yee M, Paige Lawrence B, O'Reilly MA. Lung development and the host response to influenza A virus are altered by different doses of neonatal oxygen in mice. *Am J Physiol Lung Cell Mol Physiol* 2012; 302: L1078-1087.
5. Berger J, Bhandari V. Animal models of bronchopulmonary dysplasia. The term mouse models. *Am J Physiol Lung Cell Mol Physiol* 2014; 307: L936-947.
6. Yee M, Cohen ED, Domm W, Porter GA, Jr., McDavid AN, O'Reilly MA. Neonatal hyperoxia depletes pulmonary vein cardiomyocytes in adult mice via mitochondrial oxidation. *Am J Physiol Lung Cell Mol Physiol* 2018; 314: L846-L859.
7. Yee M, Chess PR, McGrath-Morrow SA, Wang Z, Gelein R, Zhou R, Dean DA, Notter RH, O'Reilly MA. Neonatal oxygen adversely affects lung function in adult mice without altering surfactant composition or activity. *Am J Physiol Lung Cell Mol Physiol* 2009; 297: L641-649.
8. Shah D, Das P, Alam MA, Mahajan N, Romero F, Shahid M, Singh H, Bhandari V. MicroRNA-34a Promotes Endothelial Dysfunction and Mitochondrial-Mediated Apoptosis in Murine Models of Acute Lung Injury. *Am J Respir Cell Mol Biol* 2018.

9. Shah D, Romero F, Zhu Y, Duong M, Sun J, Walsh K, Summer R. C1q Deficiency Promotes Pulmonary Vascular Inflammation and Enhances the Susceptibility of the Lung Endothelium to Injury. *J Biol Chem* 2015; 290: 29642-29651.
10. Kato T, Kimura T, Ishii N, Fujii A, Yamamoto K, Kameoka S, Nishikawa T, Kasajima T. The methodology of quantitation of microvessel density and prognostic value of neovascularization associated with long-term survival in Japanese patients with breast cancer. *Breast Cancer Res Treat* 1999; 53: 19-31.
11. Shikata F, Sakaue T, Nakashiro K, Okazaki M, Kurata M, Okamura T, Okura M, Ryugo M, Nakamura Y, Yasugi T, Higashiyama S, Izutani H. Pathophysiology of lung injury induced by common bile duct ligation in mice. *PLoS One* 2014; 9: e94550.
12. James ML, Ross AC, Nicola T, Steele C, Ambalavanan N. VARA attenuates hyperoxia-induced impaired alveolar development and lung function in newborn mice. *Am J Physiol Lung Cell Mol Physiol* 2013; 304: L803-812.
13. Romero F, Shah D, Duong M, Penn RB, Fessler MB, Madenspacher J, Stafstrom W, Kavuru M, Lu B, Kallen CB, Walsh K, Summer R. A pneumocyte-macrophage paracrine lipid axis drives the lung toward fibrosis. *Am J Respir Cell Mol Biol* 2015; 53: 74-86.
14. Messier EM, Mason RJ, Kosmider B. Efficient and rapid isolation and purification of mouse alveolar type II epithelial cells. *Exp Lung Res* 2012; 38: 363-373.
15. Zhang Y, Coarfa C, Dong X, Jiang W, Hayward-Piatkovskyi B, Gleghorn JP, Lingappan K. MicroRNA-30a as a candidate underlying sex-specific differences in neonatal hyperoxic lung injury: implications for BPD. *Am J Physiol Lung Cell Mol Physiol* 2019; 316: L144-L156.
16. Oak P, Pritzke T, Thiel I, Koschlig M, Mous DS, Windhorst A, Jain N, Eickelberg O, Foerster K, Schulze A, Goepel W, Reicherzer T, Ehrhardt H, Rottier RJ, Ahnert P, Gortner L, Desai TJ, Hilgendorff A. Attenuated PDGF signaling drives alveolar and microvascular defects in neonatal chronic lung disease. *EMBO Mol Med* 2017; 9: 1504-1520.

Supplementary Figure 1

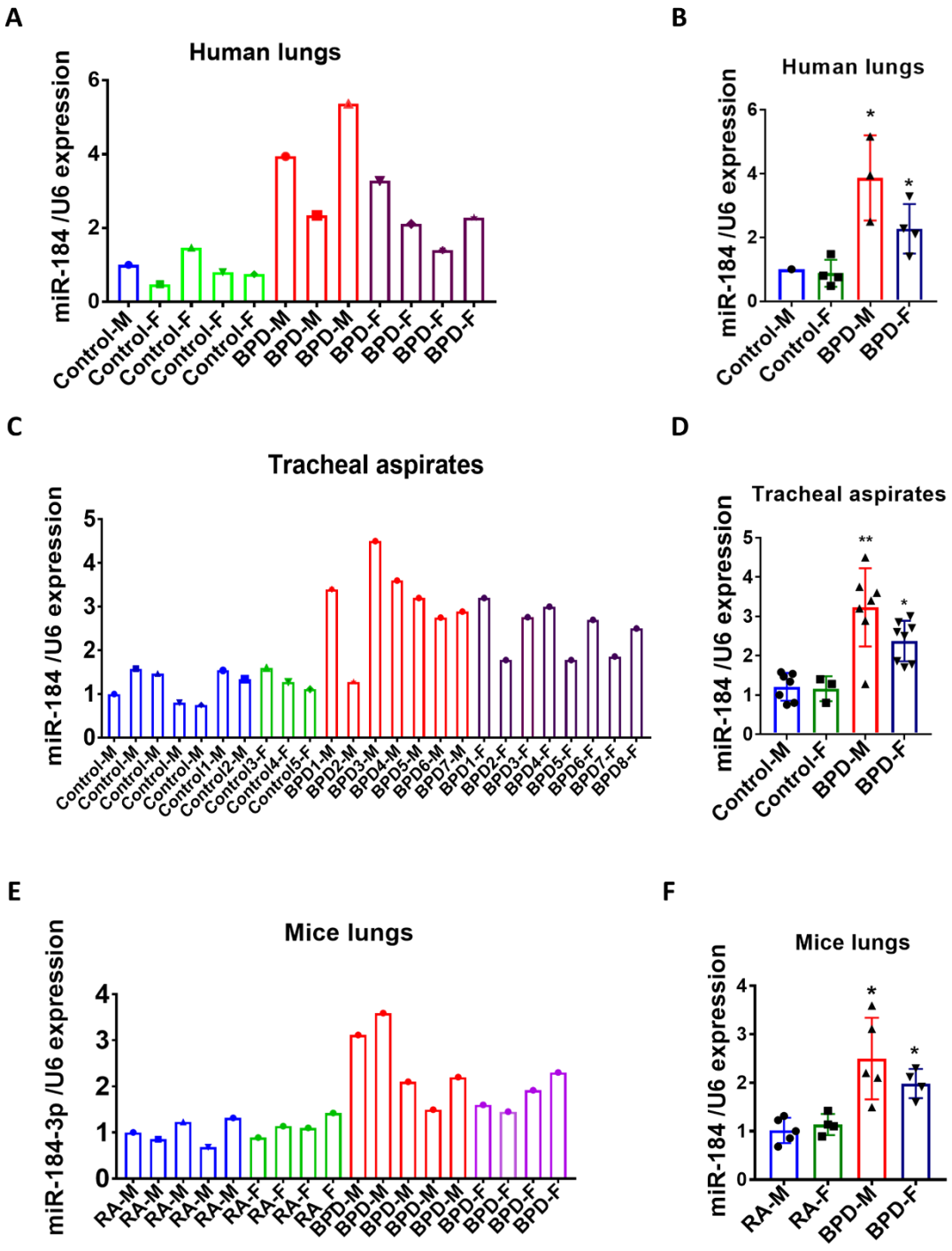

Supplementary Figure 1. Differential sex-specific expression of miR-184 expression in lungs of human neonates and murine model of experimental BPD. miR-184 expression in lungs and tracheal aspirates of male and female BPD and term controls (**A, C**) and mean value of pooled male and female controls and BPD (**B** and **D**). miR-184 expression in the male and female lungs of the murine model of experimental BPD (**E**) and mean value of pooled male and female experimental BPD mice (**F**). Data are expressed as mean ± SEM in figures B, D and F. One-way

analysis of variance (ANOVA) followed by Tukey post hoc analysis was used for statistical analyses. RA=room air, BPD= Bronchopulmonary dysplasia, M=male and F=Female

Supplementary Figure 2

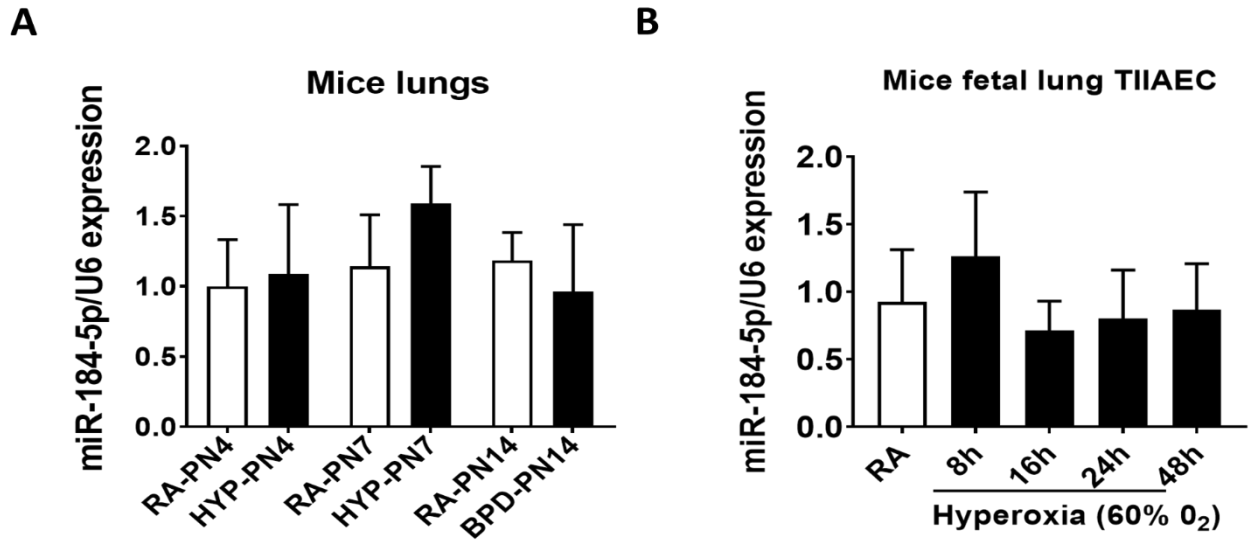

Supplementary Figure 2. miR-184-5p expression in lungs of murine model of experimental BPD. **A)** miR-184-5p levels in whole lung tissues from room air (RA, 21% O_2) and moderate hyperoxia (HYP, 60% O_2) exposure to mice till postnatal days 4 (PN4), PN7 and in BPD lungs where newborn mice were exposed to hyperoxia for first 4 days of life and then allowed to recovered in room air till PN14. **B)** miR-184-5p levels in mice fetal lung TIIAECs exposed to RA and hyperoxia at 8, 16, 24 and 48h. *In vitro* experiments were repeated 3 times and for *in vivo* experiments n=6-8 mice were used. Data are expressed as mean ± SEM. One-way analysis of variance (ANOVA) followed by Tukey post hoc analysis was used for statistical analyses.

Supplementary Figure 3

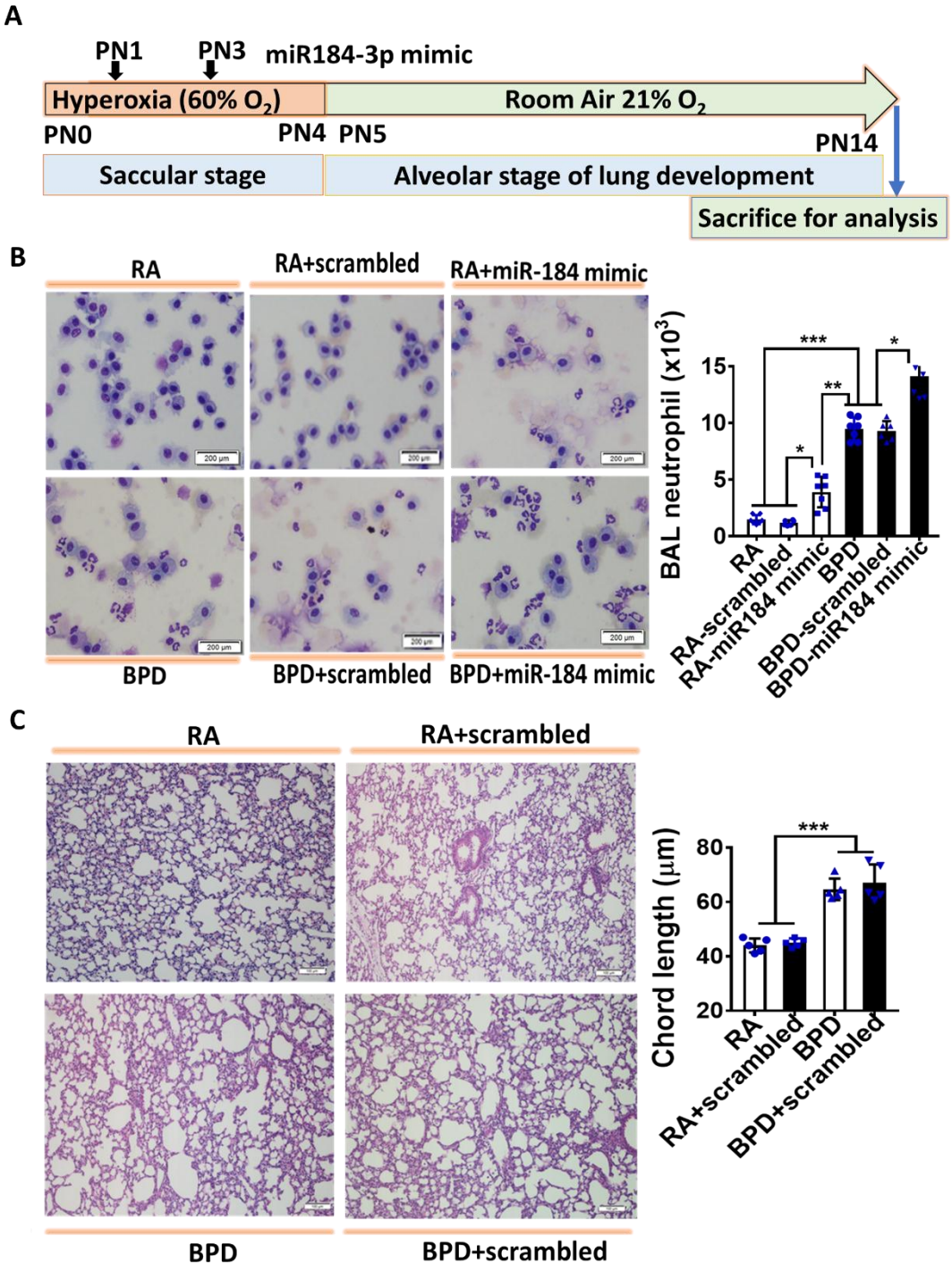

Supplementary Figure 3. A) Experimental plan for treatment newborn mice with miR-184-3-p mimic (3µl in each nostril, total dose of 20 µM) and scrambled mimic as negative control at postnatal (PN) day 1 and 3 during exposure to hyperoxia and room air (RA). **B)** Neutrophil cell counts in the BAL fluid (n=6-8 in each group, *p<0.05, **p ≤0.01 and ***p ≤0.001). **C)** Representative image of hematoxylin and eosin–stained lungs (n = 5 in each group). Scale bars: 100µm. Lung morphometric analysis measured as chord length in lungs of newborn mice treated

with or without scrambled mimic during hyperoxia or room air exposure. *p<0.05, **p ≤0.01 and ***p ≤0.001. Data are expressed as mean ± SEM.

Supplementary Figure 4

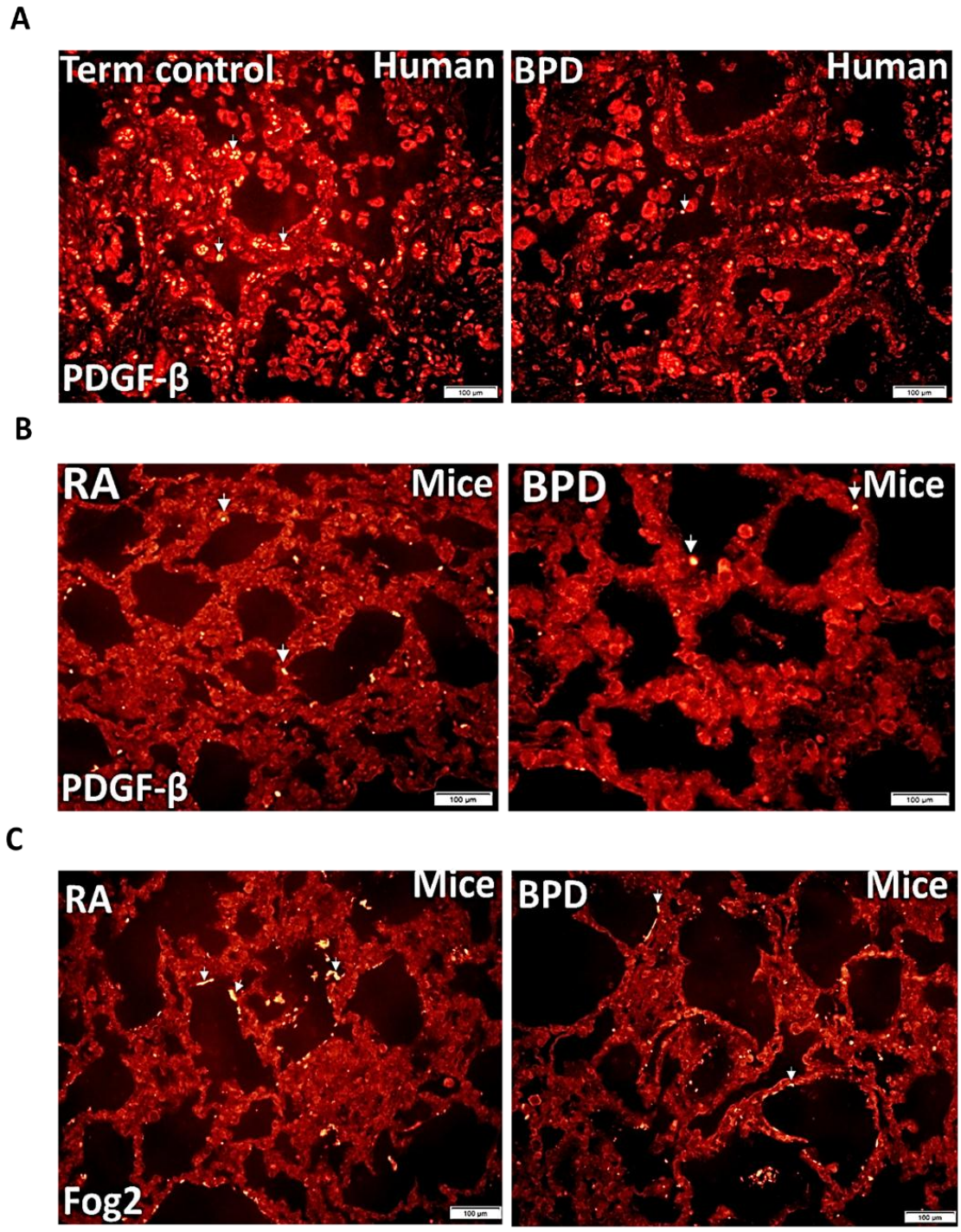

Supplementary Figure 4. PDGF-β and Fog2 expression in lungs of human BPD and murine model of hyperoxia-induced experimental BPD. **A)** Representative image of PDGF-β staining (shown as white arrows) in lungs of human neonates with BPD. **B)** Representative image of PDGF-β staining (shown as white arrows) in experimental BPD mice lungs. **C)** Representative image of Fog2 staining (shown with arrows) in lungs of murine experimental BPD. Scale bars: 100 µm.

Supplementary Figure 5

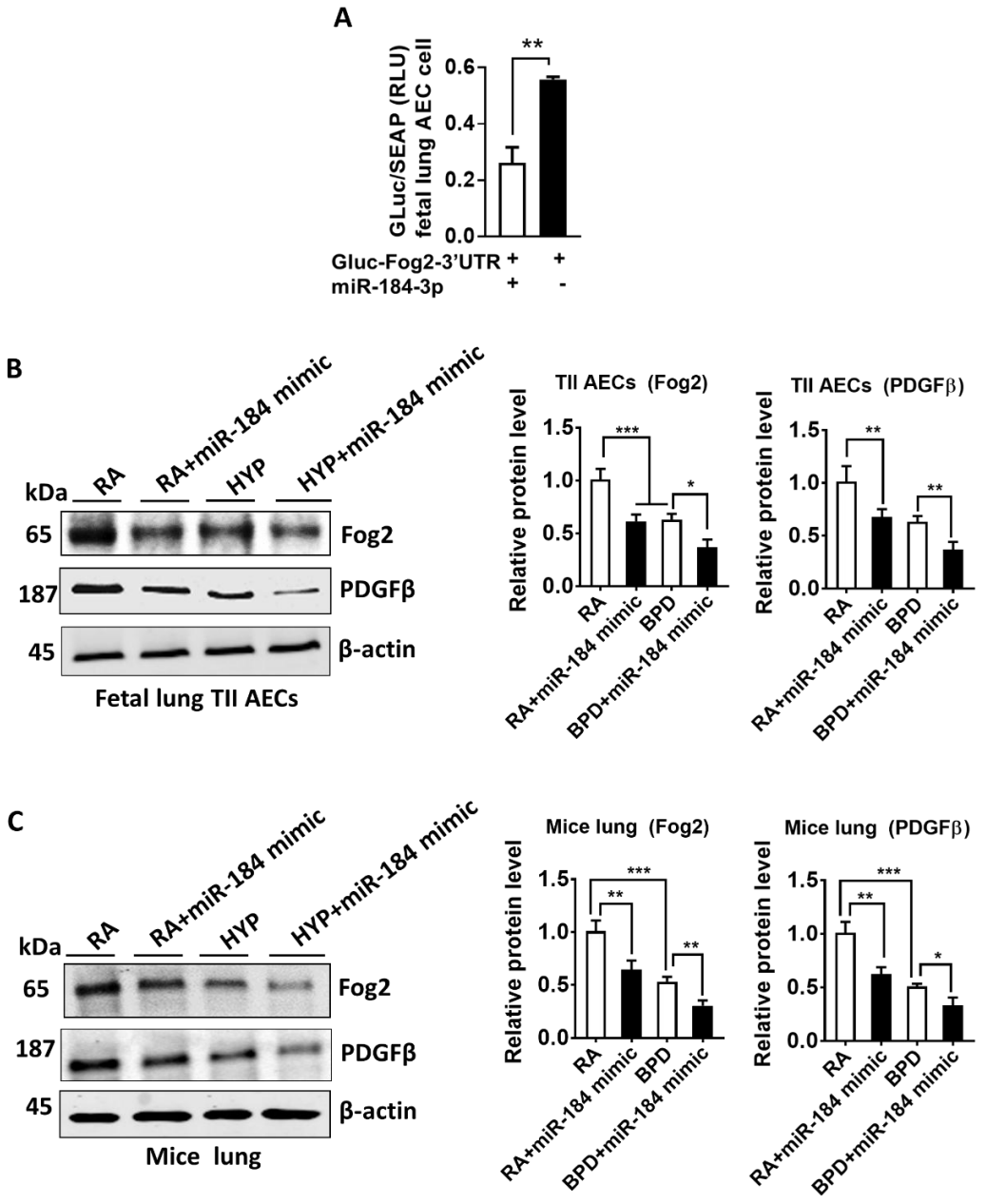

Supplementary Figure 5. miR-184-3p mimic reduces expression of PDGF-β and Fog2. **A)** mice fetal lung epithelial cells (TIIAECs) were transfected with Fog2 3'UTR (right bar) or co-transfected along with miR184-3p (left bar). Both GLuc activity and an internal control SEAP activity were determined 48h after transfection. The ratio of GLuc was normalized to SEAP. There is a significant suppression of the target gene Fog2 by miR184-3p in AECII. **B)** Western blot analysis for PDGF-β and Fog2 in fetal lung Type II alveolar epithelial cells (TIIAECs) transfected with miR-184-3p mimic (24h) and then exposed to hyperoxia (24h). Densitometric analysis shown on the right of the immunoblots (n=4 in each group, *p <0.05, **p ≤0.01 and ***p ≤0.001). Experiments were repeated twice. **C)** Western blot analysis for PDGF-β and Fog2 in lungs of RA and BPD mice treated with miR-184-3p mimic. Densitometric analysis is shown on the right of the immunoblots

(n=4-6 in each group, *p <0.05, **p ≤0.01 and ***p ≤0.001). One-way analysis of variance (ANOVA) followed by Tukey post-hoc analysis.

Supplementary Figure 6

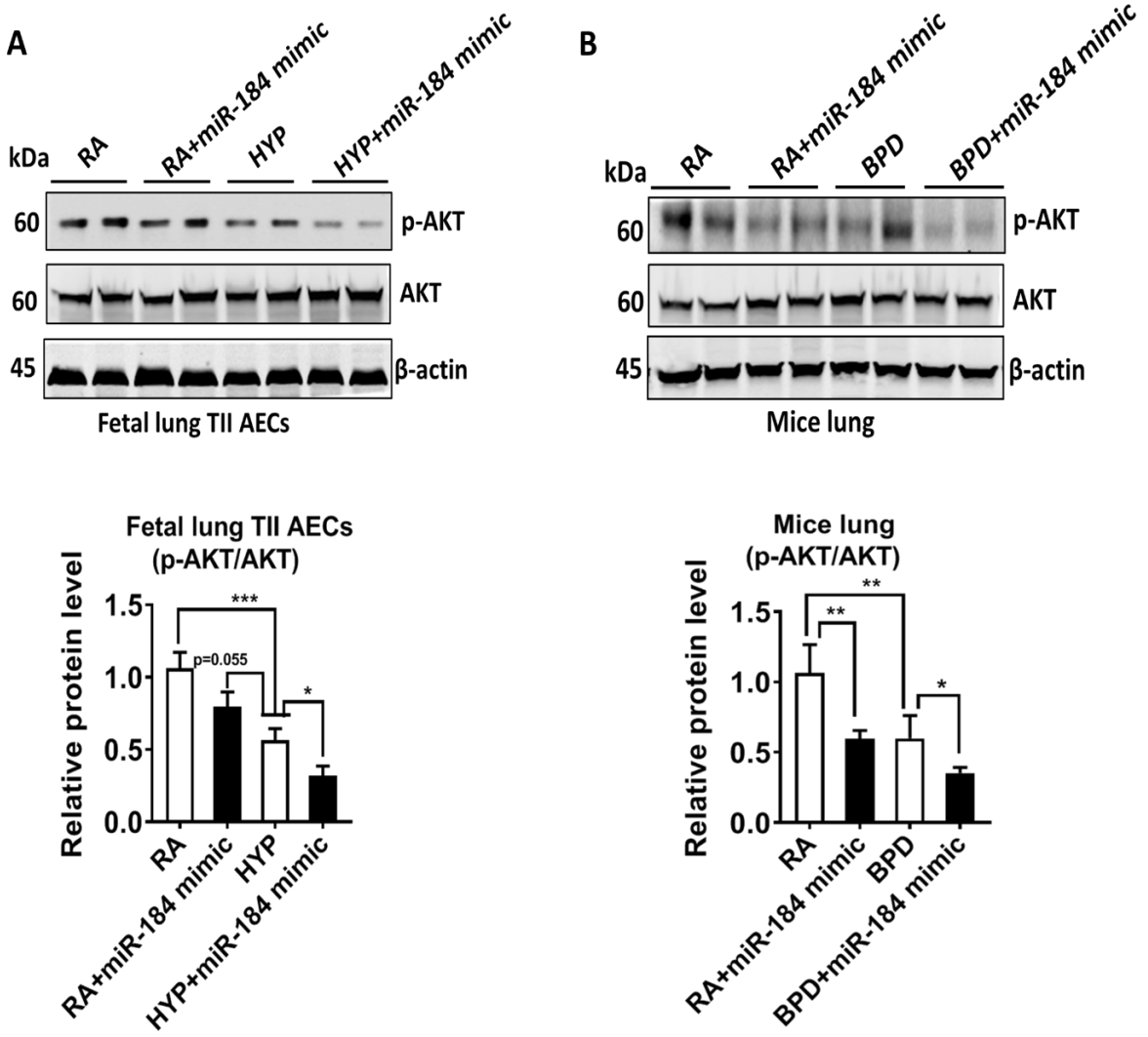

Supplementary Figure 6. A) Western blot analysis for p-AKT and AKT in fetal lung Type II alveolar epithelial cells (TIIAECs) transfected with miR-184-3p mimic (24h) and then exposed to room air (RA) or hyperoxia (HYP, 24h). Densitometric analysis is shown below the immunoblots (n=4 in each group, *p ≤0.05 and ***p ≤0.001). Experiments were repeated twice. **B)** Western blot analysis for p-AKT and AKT in lungs of room air (RA) and experimental BPD mice treated with miR-184-3p mimic. Densitometric analysis is shown below the immunoblots (n=4-6 in each group, *p ≤0.05 and **p ≤0.01). Data are expressed as mean ± SEM. One-way analysis of variance (ANOVA) followed by Tukey post hoc analysis was used for statistical analyses.

Supplementary Figure 7

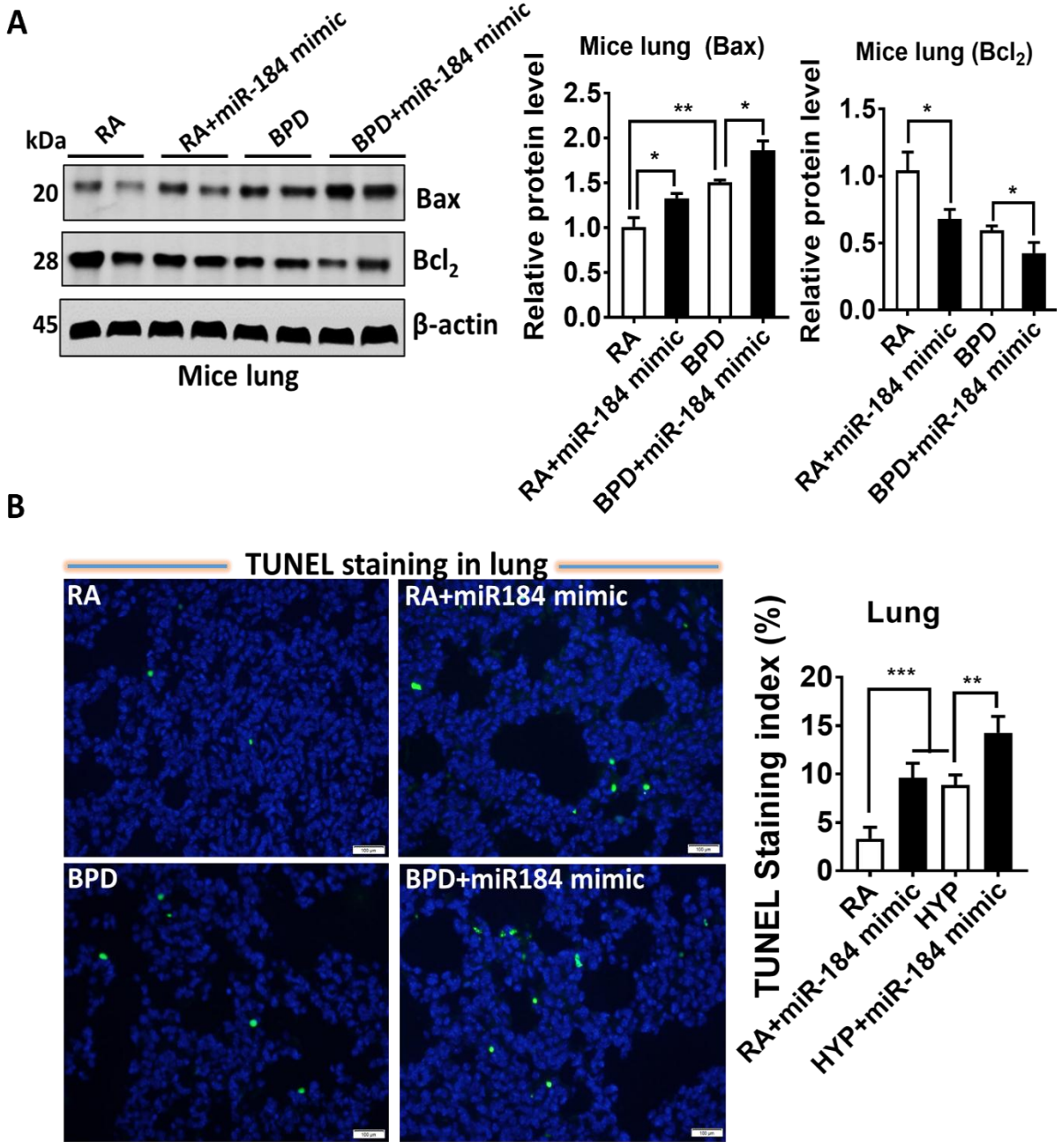

Supplementary Figure 7. A) Western blot analysis for Bax and Bcl2 in lungs of room air (RA) and experimental BPD mice treated with miR-184-3p mimic. Densitometric analysis shown to the right of the immunoblots (n=4-6 in each group, *p <0.05 and **p ≤0.01). **B)** Representative photomicrograph and quantification of TUNEL staining (green color) of apoptotic cells in lungs of RA and BPD mice transfected with miR-184-3p mimic. (n = 5 in each group, **p <0.01 and ***p ≤0.001). Scale bars: 100μm. Data are expressed as mean ± SEM.

Supplementary Figure 8

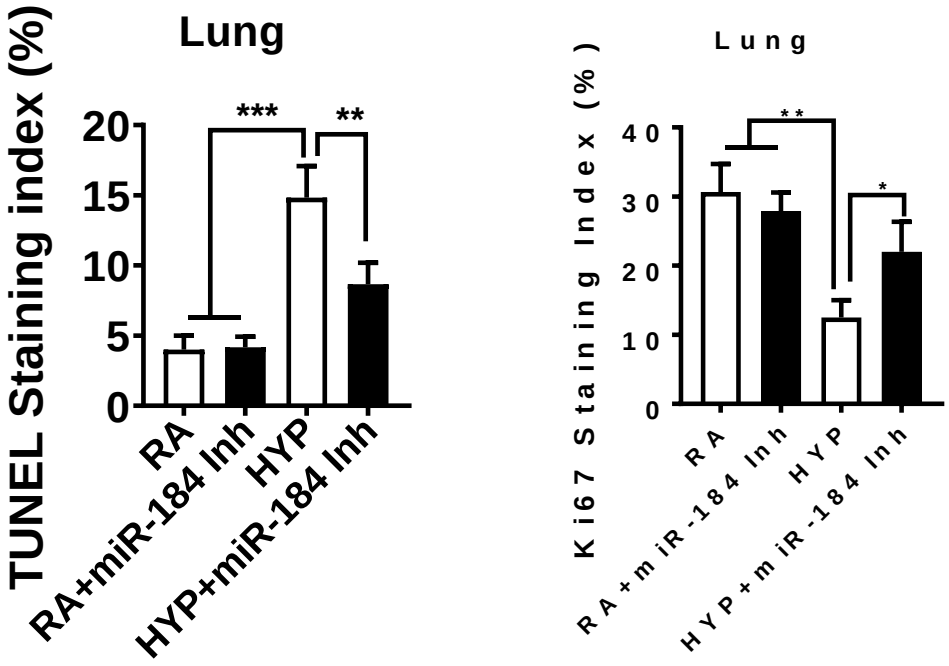

Supplementary Figure 8: A) Quantification of TUNEL staining (green color) of apoptotic cells in lungs of RA and experimental BPD mice treated with miR-184-3p inhibitor. B) Ki67 staining index (number of Ki67-positive nucle per total number of nucle, expressed as a percentage) in lungs of room air (RA) and experimental BPD mice treated with miR-184-3p inhibitor. (n = 5 in each group, *p <0.05 and **p <0.01). Scale bars: 100μm. Data are expressed as mean ± SEM.

.

Supplementary Figure 9

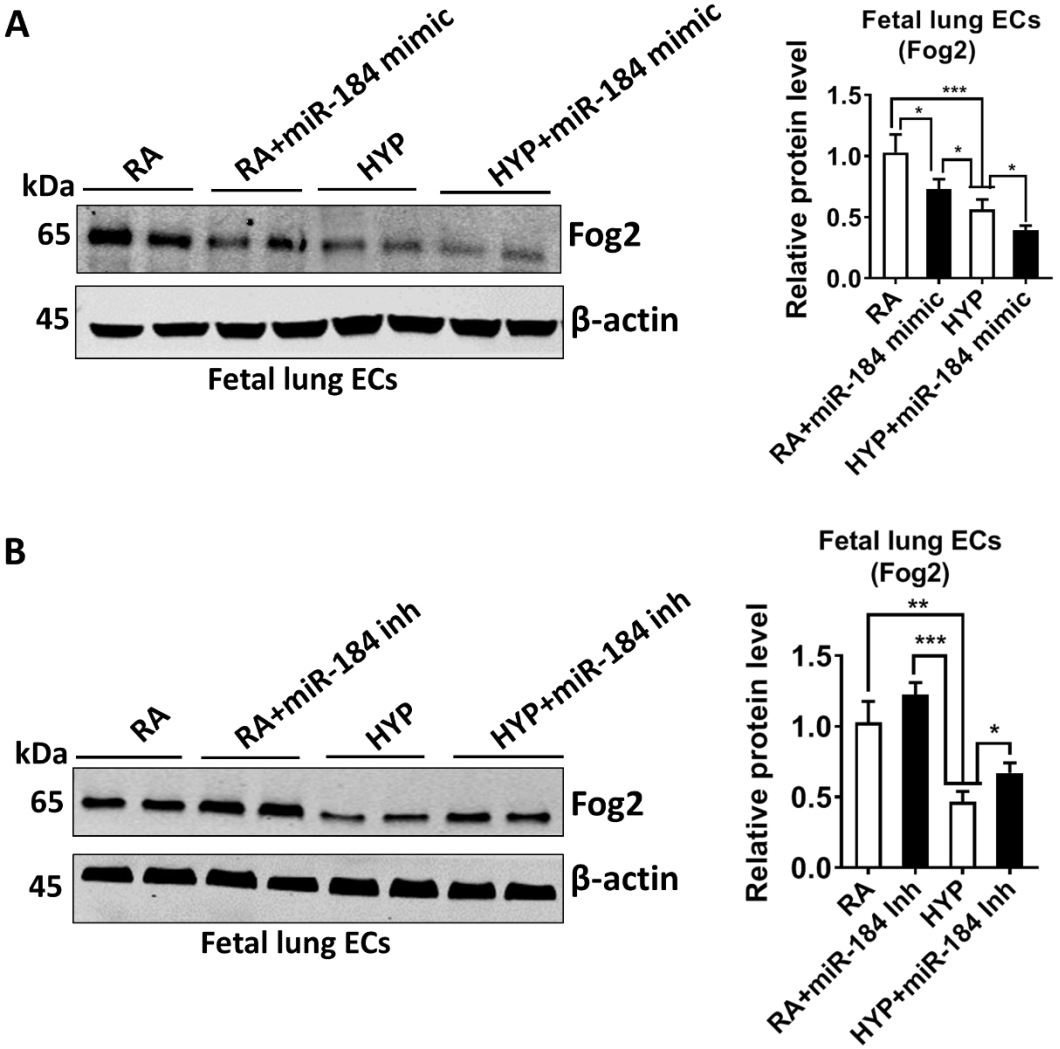

Supplementary Figure 9. A, B) Western blot analysis for Fog2 in mice fetal lung endothelial cells (ECs) transfected with miR-184-3p mimic or miR-184-3p inhibitor and exposed to room air (RA) or hyperoxia (HYP, 24h). Densitometric analysis shown next to the immunoblots (n=4 in each group, *p <0.05, **p ≤0.01 and ***p ≤0.001).

Supplementary Figure 10

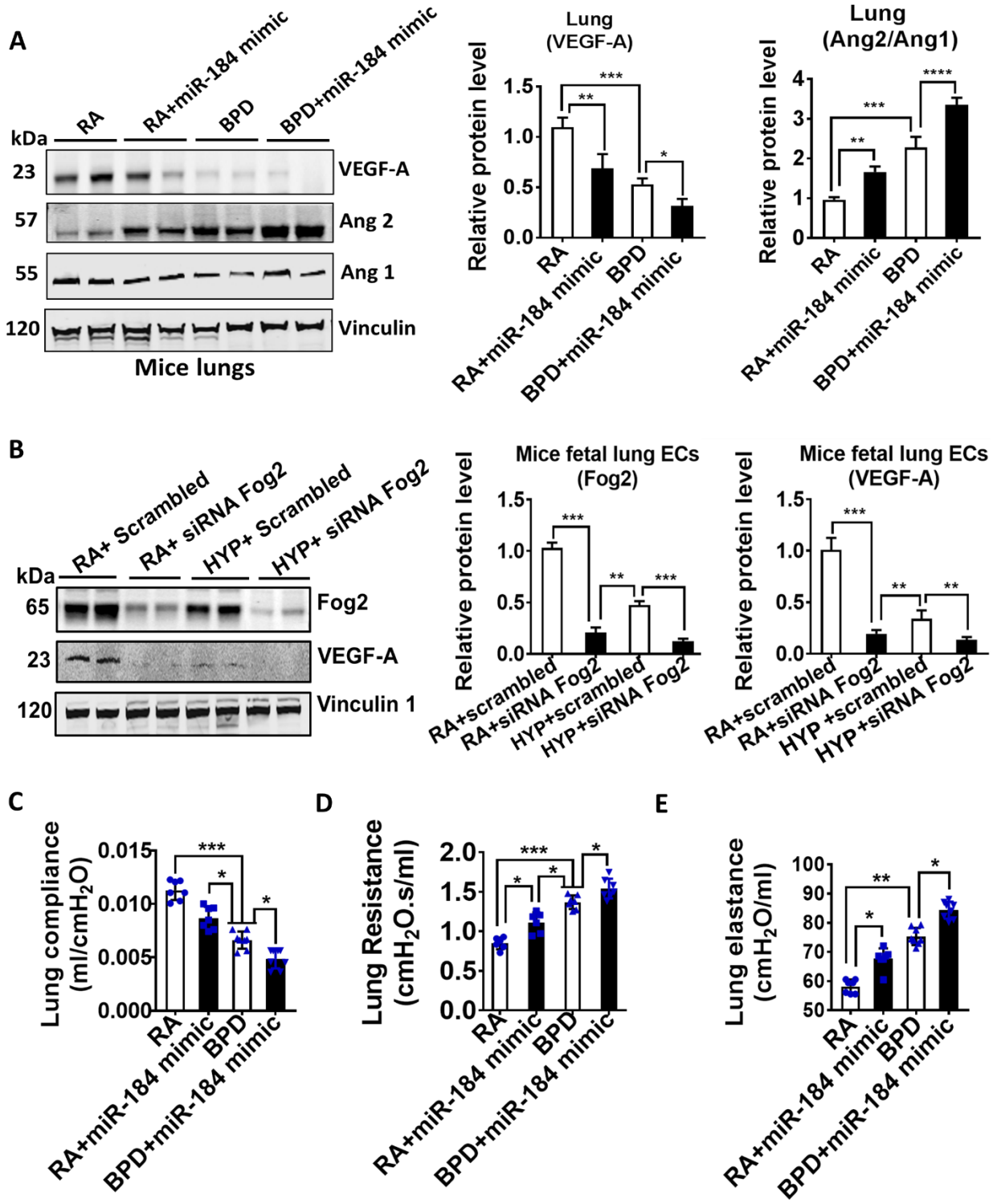

Supplementary Figure 10. A) Western blot analysis for VEGF-A, Ang2, and Ang1 in lungs of room air (RA) and BPD mice treated with miR-184-3p mimic. Densitometric analysis shown next to the immunoblots (n=4 in each group, **p ≤0.01 and ***p ≤0.001). **B)** Western blot analysis for Fog2 and VEGF-A in mice lung ECs after knockdown for Fog2 using siRNA and exposed to hyperoxia (HYP, 24h). Densitometric analysis shown next to the immunoblots (n=4 in each group, *p ≤0.05,

p ≤0.01 and ***p ≤0.001). Experiments were repeated twice. **C-E) Lung mechanics parameters measured by Flexivent (Scireq); lung compliance (Crs, n=6-8 in each group, *p ≤0.05 and ***p ≤0.001), lung resistance (Rrs, n=6-8 in each group, *p ≤0.05 and ***p ≤0.001) and lung elastance (Ers, n=6-8 in each group, *p <0.05 and **p ≤0.01).

Supplementary Figure 11

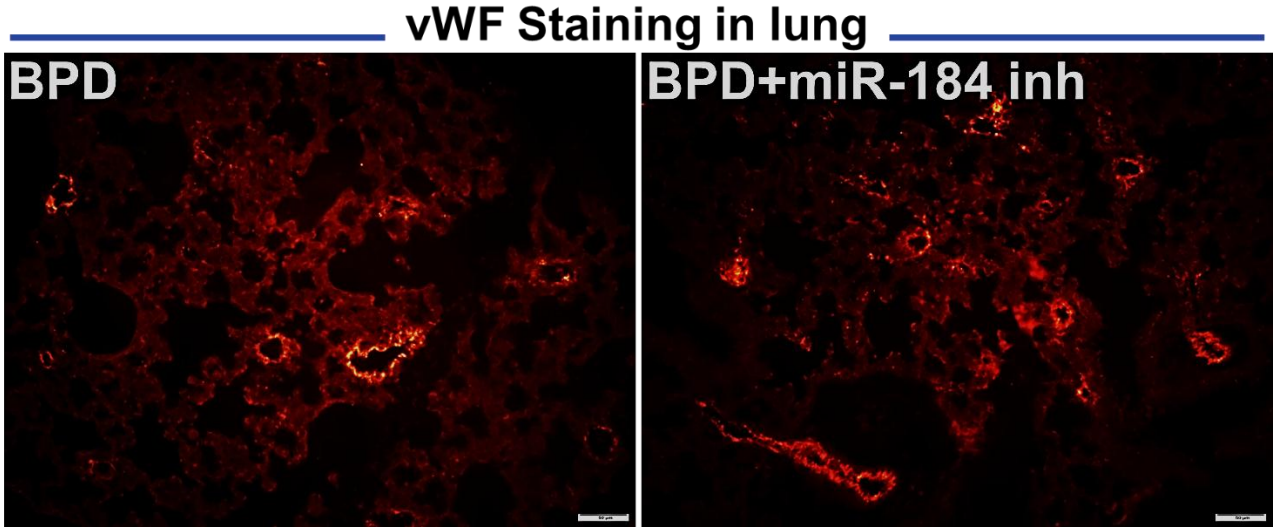

Supplementary Figure 11. Representative image of von Willebrand Factor (vWF) staining in lungs of the experimental BPD mice treated with miR-184-3p inhibitor. Quantitative evaluations of vWF fluorescence staining of at least 6 fields of view of 3 independent experiments (n = 5 in each group, *p <0.05 and **p ≤0.01).

Supplemental Table E1: Selected clinical data of infants whose tracheal aspirates were used to detect miR184 expression (**Figs. 1A and Supplementary Figs. 1C and 1D**).

Gestational Age (weeks)	Sex	Birth weight (g)	Days at sample collection	Final Outcome
24	Female	610	6	**BPD**
25	Male	630	3	**BPD**
24	Male	629	5	**BPD**
24	Male	580	4	**BPD**
25	Female	620	3	**BPD**
25	Female	645	6	**BPD**
25	Female	633	5	**BPD**
25	Female	680	5	**BPD**
27	Male	1060	5	**BPD**
27	Male	850	6	**BPD**
23	Male	435	5	**BPD**
25	Male	706	7	**BPD**
24	Female	680	7	**BPD**
25	Female	697	7	**BPD**
24	Female	689	5	**BPD**
27	Male	1049	3	**No BPD**
27	Male	925	2	**No BPD**
27	Female	1049	3	**No BPD**
27	Female	1011	4	**No BPD**
27	Female	930	3	**No BPD**
26	Male	724	5	**No BPD**
24	Male	610	3	**No BPD**
24	Male	610	4	**No BPD**
26	Male	710	3	**No BPD**
26	Male	765	3	**No BPD**

BPD: bronchopulmonary dysplasia

Supplemental Table E2: Selected clinical data of infants whose lungs were used to detect miR-184, PDGF-β and Fog2 expression (**Figs. 1B, 5A**, **Supplementary Figs. 1A and 1B**)

Sample ID	Sex	Laboratory Diagnosis	LOS (days)	On Vent (days)	Time on O_2 >0.5 (hours/days)	Time on O_2 >0.21, <0.5 (hours/days)	NICU Diagnoses	Gestational age at birth (weeks)	Birth weight (grams)
4	Female	None (Term)	3	2	1-2h	1h	Nonketotic Hyperglycinemia; Abnl EEG-seizures	41	3480
8	Female	None (Term)	4	1	2h	1D	Pena-Shokeir Phenotype; ?Spinal Muscular Atrophy	40	2035
21	Female	None (Term)	1	2	2D	0	HIE; Hypoglycemia; Burst Suppression EEG	36	2580
30	Male	None (Term)	1	2	1-2h	1-2h	Perinatal Asphyxia	38.5	3560
50	Female	None (Term)	3	3	0	3D	Severe HIE	41	4300
10	Male	BPD	12	13	13	35	BPD; IVH-G4&3; PDA	26	1021
11	Female	BPD	57	32	23	24	Severe BPD; NEC (no pneumatosis)	26	910
14	Female	BPD	17	18	7	11	BPS; PDA; Sepsis; NEC	26	620
17	Male	BPD	64	62	30	35	BPD; CMV	25	520
18	Male	BPD	96	97	96	1	BPD; PVL; UTI	27	825
33	Female	BPD	97	57	23	73	BPD; SGA; CMV; PH	29.2	520
44	Male	BPD	119	95	13	107	BPD; PDA; possible sepsis	28	965

Vent: invasive ventilation; RA: room air; N/A: Information not available; CPAP: continuous positive airway pressure; BPD: bronchopulmonary dysplasia; HIE: Hypoxic-Ischemic Encephalopathy; EEG: electroencephalogram; IVH: Intraventricular hemorrhage; PDA: Patent ductus arteriosus; NEC: Necrotizing enterocolitis; CMV: Cytomegalovirus; PVL; Periventricular leukomalacia; UTI: Urinary tract infection; SGA: Small for gestational age; PH; Pulmonary Hypertension

Supplemental Table E3: Selected clinical data of infants whose lungs were used for Pdgf-β immunohistochemical staining (**Supplemental Fig. 4A and 4B**).

Diagnosis	**Sex**	**Gestational Age (weeks)**	**Birth weight (grams)**	**Age at death (days)**
BPD	Male	26+6	890	79
BPD	Male	29	765	125
Term control	Female	41	4300	3
Term control	Male	37	2800	4 hours

BPD: bronchopulmonary dysplasia